Chromatin accessibility profiling reveals that human fibroblasts respond to mechanical stimulation in a cell specific manner

Niall J Logan
Imperial College London
Nikolaos Pantelireis
Imperial College London
Marie Camman
Imperial College London
Greg Williams
Farjo Hair Institute
Claire A Higgins (c.higgins@imperial.ac.uk)
Imperial College London

Research Article

Keywords: ATAC-seq, RNA-seq, osteogenic differentiation, fibroblast heterogeneity, chromatin accessibility

Posted Date: May 4th, 2021

DOI: https://doi.org/10.21203/rs.3.rs-471016/v1

Chromatin accessibility profiling reveals that human fibroblasts respond to mechanical stimulation in a cell specific manner

Niall J Logan [1], Nikolaos Pantelireis [1], Marie Camman [1], Greg Williams [2], Claire A Higgins [1]*

[1] Department of Bioengineering,
Imperial College London
London,
SW7 2AZ,
United Kingdom

[2] Farjo Hair Institute,
70 Quay Street,
Manchester,
M3 3EJ,
United Kingdom

* Corresponding Author
Claire A Higgins
Department of Bioengineering,
Imperial College London
London,
SW7 2AZ,
United Kingdom
Email: c.higgins@imperial.ac.uk
Phone: +442075945826

Abstract:

- **Background:** Fibroblasts in the skin are highly heterogeneous, both in vivo and in vitro. One intriguing difference between follicular and interfollicular fibroblasts in vitro is their ability to differentiate in response to osteogenic media, or mechanical stimulation. In this study, we asked whether differences in the ability to respond to differentiation stimuli are due to baseline differences in chromatin accessibility.
- **Results:** We performed chromatin accessibility and transcriptional profiling of two fibroblast subtypes found in human skin, which arise from a common progenitor during development yet display distinct characteristics in adult tissue and in vitro. We found that when cells were grown in regular growth media (GM) in culture they had unique chromatin accessibility profiles, however, these profiles control similar functional networks. When we introduced a chemical perturbation and grew cells in osteogenic media (OM) to promote differentiation, we observed a divergence not only in the accessible chromatin signatures but also in the functional networks controlled by these signatures. The biggest divergence was observed when we applied two perturbations to cells; growth in OM combined with mechanical stimulation in the form of a shock wave (OMSW). Here, in one of the fibroblast subtypes we found a number of uniquely accessible promoters which controlled osteogenic interaction networks associated with bone and differentiation functions. This fibroblast subtype also readily differentiates into bone in OMSW conditions, while the other fibroblast subtype under analysis lacks differentiation capability *in vitro*.
- **Conclusions:** Using ATAC-seq and RNA-seq we found that a combination of two stimuli could result significant and specific changes in chromatin accessibility associated with osteogenic differentiation, but only within the fibroblast sub-type capable of osteogenic differentiation. Our results suggest that these two stimuli elicit this cell specific response by modifying chromatin accessibility of osteogenic related gene promoters.

Keywords: ATAC-seq, RNA-seq, osteogenic differentiation, fibroblast heterogeneity, chromatin accessibility

Background

Phenotypic behaviour of a cell can be traced back to the genomic level where chromatin organisation can influence accessibility to genomic regions and affect biological processes. Recent advances in next generation sequencing [1] now allow for epigenetic mapping of the genome and have been used to help answer fundamental questions relating to the role of chromatin organisation in biological processes such as cell differentiation [2-4], development [5, 6], and plasticity [7].

Here, we applied these technologies to investigate differences between skin fibroblasts, which display both inter and intra-location heterogeneity [8]. Lineage tracing studies have revealed that a fibroblast subtype found in the hair follicle, dermal papilla (DP) fibroblasts, share a common developmental progenitor with an interfollicular subtype, papillary fibroblasts (PFi) [9]. Despite arising from the same developmental progenitor [9], DP and PFi have distinct identities both *in vivo* and *in vitro*; DP cells can differentiate down osteogenic [10, 11] and adipogenic [11, 12] linages *in vitro*, while PFi lack this differentiation capacity [13]. DP and PFi also differ in their response to mechanical stimuli, and we previously demonstrated that mechanical stimulation of cells in culture (in the form of a single 165 kPa shock wave (SW) in air) in combination with osteogenic media (OM), resulted in enhanced and accelerated osteogenic differentiation of DP, whereas PFi were unresponsive to this stimuli [13]. It is important to note that the SW alone could not promote ossification of DP, but rather it acted in a synergistic manner with OM, accelerating and enhancing mineral deposition in follicular derived DP cells [13].

Based on the above, we hypothesised that external chemical stimuli, such as introduction of osteogenic differentiation media, or mechanical stimuli, elicit a differential response in fibroblast

subtypes due to differences in in chromatin accessibility. To test this, we performed next generation sequencing to assess both chromatin accessibility and transcriptional profiles in cells. Assay for transposase accessible chromatin in combination with high throughput sequencing (ATAC-seq) is a technique that utilises a genetically engineered hyperactive Tn5 transposase to tag and ligate fragments from regions of accessible chromatin throughout the genome [14]. In combination with ATAC-seq we performed RNA-sequencing (RNA-seq) to evaluate if the accessibility of chromatin regions could be correlated with changes to transcriptional activity occurring in PFi and DP cells. Sequencing was initially performed on both fibroblast subtypes (DP and PFi) in growth media (GM) to establish baseline differences between cells. We then introduced two perturbations; a chemical one in the form of OM alone, and a second one which combined OM together with mechanical stimulation in the form of a shock wave (OMSW). While fibroblast subtypes displayed similarities in chromatin organisation in GM, we found that the double perturbation resulted in a cell specific response, with two distinct chromatin accessibility profiles with unique ontology signatures emerging. Specifically, within the DP cells, which we know have enhanced osteogenic differentiation capability in OMSW, we found that open chromatin was associated with an enrichment of osteogenic gene networks that were not present in any other cell type or condition. This indicates that chromatin rearrangements in response to external stimuli can occur in a cell specific manner, and helps to explain the divergent response of DP and PFi to differentiation stimuli *in vitro.*

Results

PFi and DP cells share similar chromatin organisation in GM conditions

Previous work shows that DP cells, but not PFi, will readily differentiate down an osteogenic lineage *in vitro* [13], however it is not known if this is due to baseline differences in the epigenetic landscape between each cell type. To ascertain the baseline landscape, and determine if DP are pre-sensitised to differentiate down an osteogenic lineage in vitro, we assessed both the chromatin accessibility and transcriptional profiles of each cell type in GM,

ATAC-seq and RNA-seq libraries were generated from DP and PFi cells grown in GM, with DNA and RNA isolated 48 hours after cell seeding. Early insert size analysis of ATAC-seq libraries showed the clear presence of a banding pattern, associated with nucleosome positioning of the transposase and correlating with high quality libraries [14] (Fig. 1a, Fig. S1). Post sequencing quality checks showed an appropriate distribution of the number of called peaks (Fig. 1b) between the biological replicates, which correlated with high fragments of reads in peaks (FRiP) scores greater than 0.35 (Fig. 1c). Concordance between the two sets of biological replicates was high, and reported as 0.96 and 0.88 for PFi and DP (Fig. 1d) respectively, therefore replicates were merged for further analysis. A comparative analysis was then performed to identify peaks unique to either PFi or DP, referred to as condition specific peaks. While 182070 peaks were shared between the cell types, 196675 peaks were unique to PFi and 143065 were unique to DP cells (Fig. 1e). As chromatin accessibility around transcription start sites (TSS) can affect transcription factor binding, this can ultimately lead to altered downstream transcriptional activity [15]. We therefore decided to narrow our focus and filter the condition specific peaks from each cell type, for peaks that were identified within 3000bp of TSSs (referred to hereon in as promoter peaks). Peak annotation showed that the distribution of peaks was similar between the cell types (Fig. 1f) with 9.0 and 9.5% of peaks falling within the promoter regions of PFi and DP cells, respectively. As multiple peaks can fall within a single promoter, we performed a Venn analysis to acquire gene lists of unique and shared promoters containing at least one condition specific peak in either PFi or DP, identifying 2602 in PFi, and 3831 in DP (Fig. 1g). Using these lists, we performed gene ontology analysis using Ingenuity Pathway Analysis (IPA) core analyses. Despite identifying unique promoter peaks for each cell type, the ontology analysis revealed high similarities between cell types, with regard to the types of networks these peaks were present in (Fig. 1h). Four of the top five 'physiological system development and functions' identified were shared between DP and PFi, implying that even though there are distinct chromatin accessibility landscapes in each cell type, the overcasting function of the genes regulated by the altered chromatin state were remarkably similar.

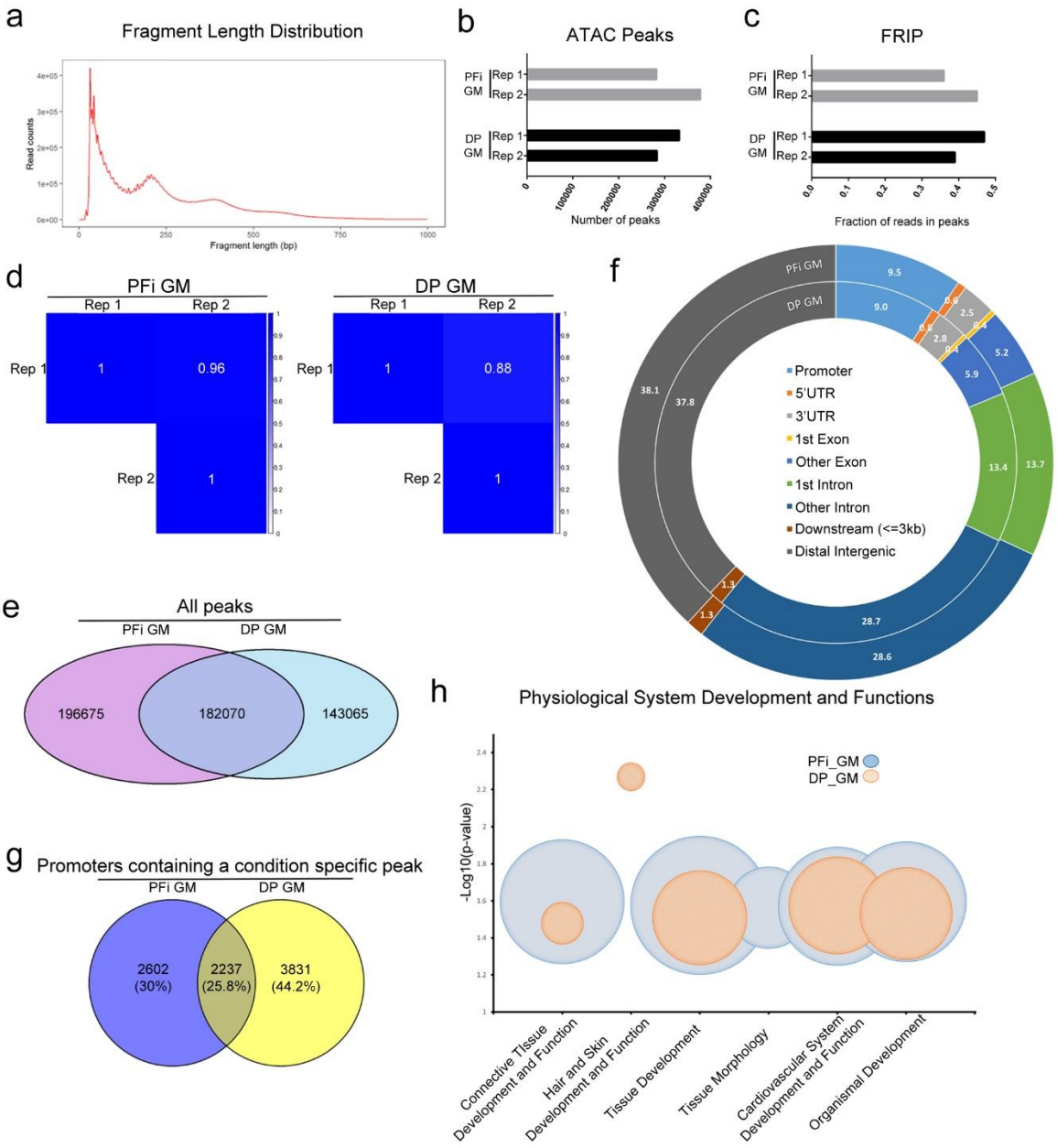

Figure 1. GM Comparison of ATAC-seq data shows similarities between fibroblast subtypes; a) ATAC-seq nucleosome banding on PFi GM library; b) Number of ATAC peaks in individual biological replicates; c) FRiP scores from individual biological replicates; d) Correlation matrix; e) Venn diagram displaying crossover of all ATAC peaks in each condition; f) Peak annotation of specific ATAC peaks on merged samples; g) Venn diagram displaying gene promoters in each condition; h) Gene ontology analysis on ATAC data generated using IPA core analyses. The size of the bubble represents the number of molecules associated within that function.

Using IPA to identify ontology terms over-represented in either DP or PFi as described above, we identified only one unique function in DP cells, specifically associated with 'hair and skin development and function'. This is of particular interest considering the known role that DP play in hair development and cycling. These cells, both *in vivo* and *in vitro*, are capable of instructing new hair follicle development, while PFi lack this capacity [16].

In addition to generating ATAC-Seq data, we also performed RNA-seq analysis in order to obtain baseline transcriptional signatures for DP and PFi. Using DESeq2 to identify genes which were significantly ($p \leq 0.05$, false discovery rate (FDR) ≤ 0.01) and differentially expressed between the two cell types, we identified 310 genes upregulated in DP and 258 genes upregulated in PFi, compared to the other cell type (Fig. 2a,b). Ontology of upregulated genes in each cell type was performed using the Panther overrepresentation test which looks at the representation of an ontology term in a given gene list compared to representation of that term in the whole genome [17]. For PFi, only 3 ontology terms were identified as overrepresented compared to 19 for DP. Of the 3 PFi terms, 2 terms - 'mesoderm development' and 'developmental process' - were shared with DP, while only 1 term – 'cell differentiation' - was unique. The upregulated genes identified in DP cells, had overrepresentation of a variety of terms, including 'cell adhesion' and 'cytoskeletal organization' (Fig. 2c). Notably lacking from the DP ontology analysis were any terms associated with osteogenic differentiation, suggesting that the DP cells are not primed to differentiate in response to the introduction of osteogenic media.

To ascertain if there was any correlation between transcriptional activity and chromatin accessibility in PFi and DP cells in GM, we performed a Venn analysis to cross compare our RNA-seq gene lists and the ATAC-seq lists used in the earlier ontology analysis (Fig. 2d). Of the 568 differentially expressed genes, 251 had been previously identified in by our promoter specific peak ATAC-seq analysis (Fig. 1g). When we focused on the DP cells, 108 genes contained uniquely open chromatin in their promoters and also showed differential expression between DP and PFi. Of these, 63% of the

159 genes were also upregulated in DP, indicating that enhanced transcriptional activity of these genes is
160 associated with the presence of a condition specific peak in their promoters (Fig. 2e). With PFi, 73
161 genes which were differentially regulated at the transcriptional level regulated also contained
162 condition specific ATAC-Seq promoter peaks, with 70% of these showing an increase in RNA
163 transcription For example podoplanin (*PDPN*), which is a well described marker of PFi both *in vivo*
164 and *in vitro* [18] has accessible chromatin uniquely in PFi, and is only transcribed in PFi (Fig. 2f). This
165 data demonstrates that in general, the presence of a condition specific ATAC peak within the
166 promoter region of a gene is positively correlated with increased transcriptional activity.

167 We initially set out to determine baseline differences between DP and PFi, to help explain why we
168 observe a differential response to perturbation of these cells in culture. Despite identifying unique
169 chromatin accessibility profiles between cells, we found that the overarching physiological functions
170 controlled by these open chromatin gene lists were relatively similar. This suggests that the
171 differential response of cells in differentiation conditions is not due to baseline differences in
172 chromatin architecture, and that DP cells are not epigenetically primed to differentiate into an
173 osteogenic lineage.

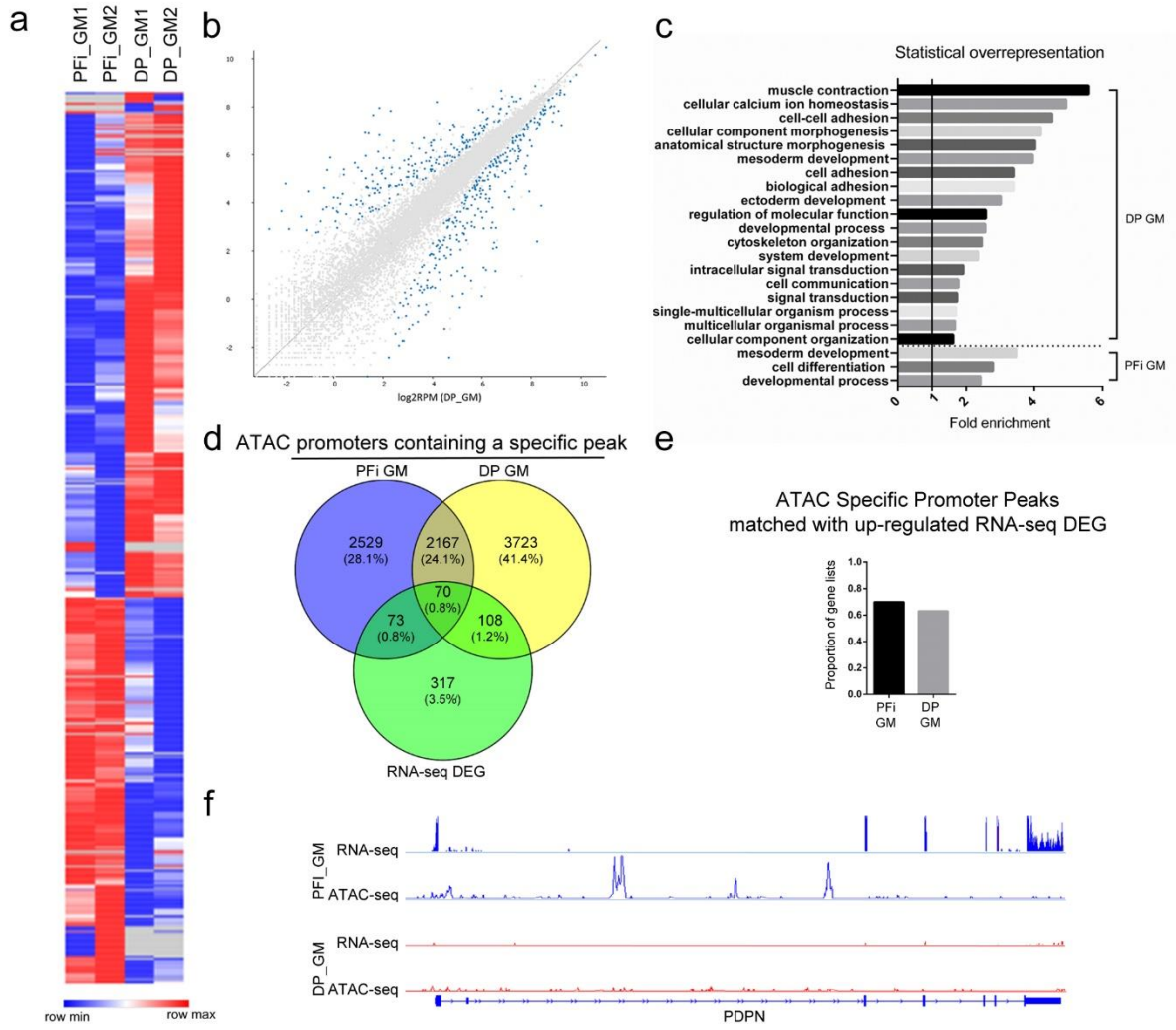

Figure 2. GM Comparison of RNA-seq and ATAC-seq data shows similarities between fibroblast subtypes; a) Heat map displaying differentially expressed genes from RNA-seq analysis; b) Scatter plot showing distribution of RNA-seq differentially expressed genes (blue); c) Gene ontology showing statistically over/under-represented biological processes from upregulated genes in each cell type; d) Venn displaying correlation of ATAC promoters and RNA-seq differentially expressed genes; e) Proportion of ATAC promoters that match with upregulated expression in RNA-seq data; f) Example of RNA-seq differentially expressed gene matched with identification of an ATAC specific peak within its promoters. Gene shown: *PDPN*.

185 *DP and PFi in OM start to diverge at the transcriptional level*

186 Despite DP and PFi cells in GM each possessing a unique chromatin accessibility profile of gene
187 promoters, our analysis so far demonstrated that the overcasting functions of these individual
188 landscapes were for the most part, overlapping. As both DP and PFi are fibroblast subtypes found in
189 the skin dermis and originate from the same progenitor [9], similarities between these two cell
190 populations can be expected. However, as PFi cells do not share the same differentiation capacity as
191 DP cells [13], we wanted to know if the introduction of a single chemical perturbation in the form of
192 OM would result in differential changes in chromatin accessibility between fibroblast subtypes, or if
193 transcriptional changes alone are driving the osteogenic differentiation of DP cells [10, 11].

194 To answer this, we performed ATAC-Seq and RNA-Seq on DP and PFi grown in OM for 24 hours. This
195 early time point was selected as we wanted to identify changes associated with the initial
196 introduction of OM, rather than changes associated with deposition of mineral (ossification) which
197 occurs several days later. As with the GM ATAC libraries, a clear banding pattern [14] was visible on
198 all OM samples from insert size analysis (Fig. 3a, Fig. S1), while the number of called peaks was well
199 distributed amongst biological replicate sets (Fig. 3b) producing FRiP scores greater than 0.3 (Fig. 3c).
200 Biological replicates showed a high extent of concordance, reported as 0.92 and 0.93 for PFi and DP
201 in OM, respectively (Fig. 3d), and were merged for further downstream analysis. A comparative
202 analysis to identify condition specific peaks found that 201375 peaks were shared between both cell
203 types, whilst 206451 peaks were unique to PFi OM and 158995 were unique to the DP OM condition
204 (Fig. 3e). Of these called peaks, 9.2% and 8.5% fell within the promoter region of PFi and DP,
205 respectively (Fig. 3f). After identifying genes associated with these promoters, we performed a Venn
206 analysis to acquire a list of 2669 genes unique to PFi, and 3772 in DP (Fig. 3g), and used these lists to
207 perform ontology analysis in IPA. In contrast to the ontology analysis performed on cells in GM, this
208 time, only two of the top five physiological system development and functions identified were
209 common to both cell types (Fig. 3h). The other identified functions were unique to the top 5 list of

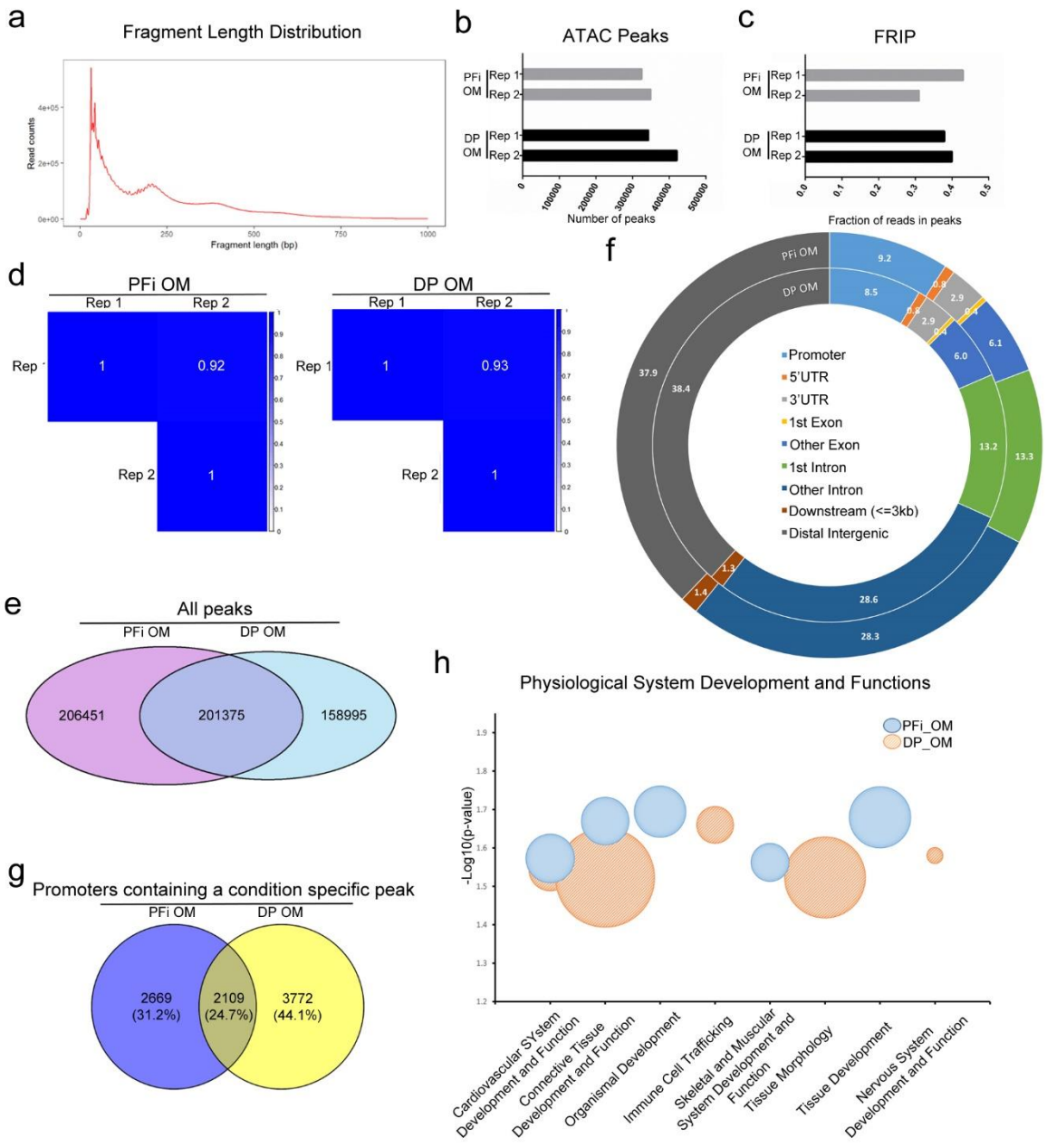

Figure 3. OM Comparison of ATAC-seq reveals divergence of physiological system development and functions; a) ATAC-seq nucleosome banding on PFi OM library; b) Number of ATAC peaks in individual biological replicates; c) FRiP scores from individual biological replicates; d) Correlation matrix; e) Venn diagram displaying crossover of all ATAC peaks in each condition; f) Peak annotation of specific ATAC peaks on merged samples; g) Venn diagram displaying gene promoters in each condition; h) Gene ontology analysis on ATAC data generated using IPA core analyses. The size of the bubble represents the number of molecules associated within that function.

either DP or PFi (Fig. 2h), suggesting that the chromatin accessibility profiles of cells are starting to diverge. However, none of the identified functions were related to osteogenic differentiation, suggesting that accessibility of chromatin may not be what is driving the osteogenic response of DP cells in OM.

In addition to the ATAC analysis, RNA-seq was performed on DP and PFi in OM, enabling identification of 455 and 398 genes that were upregulated respectively in DP and PFi (Fig. 4a,b). Statistical overrepresentation testing using Panther [17], found 22 terms overrepresented in the DP OM gene list. This included 17 of the 19 terms previous identified in the DP GM list (Fig. 2c), suggesting identification of a DP specific gene signature regardless of the culture media. Intriguingly, the most significantly overrepresented ontology term in the DP OM (Fig. 4c), was 'skeletal system development', which has daughter terms including 'bone cell development', 'ossification involved in bone maturation' and 'mesenchymal cell differentiation involved in bone development'. In PFi OM, 18 ontology terms were also overrepresented, including a number associated with 'metabolic processes', 'cell cycle' and 'DNA replication'. Despite both the PFi and DP cells being grown in OM for 24 hours, there were no terms associated with osteogenic differentiation identified in the PFi dataset.

Lastly, we wanted to assess if there was any correlation between our ATAC-seq OM chromatin accessibility profiles and our OM differentially expressed gene lists. We found that of 853 differentially expressed genes, 334 were also identified as having condition specific open chromatin at their promoters (Fig. 4d). Similar to the GM analysis, of the genes that did correlate between RNA and ATAC lists, we found that 60% and 72% of genes respectively in PFi and DP, showed an upregulation in transcriptional actively with the presence of a condition specific peak located within the promoter region of the target gene (Fig. 4e). For example, we found that osteopontin, also known as secreted phosphoprotein 1 (*OPN, SPP1*) was not only upregulated in DP cells, but also had a condition specific peak within its promoter (Fig. 4f). SPP1 has a well-known role in bone formation,

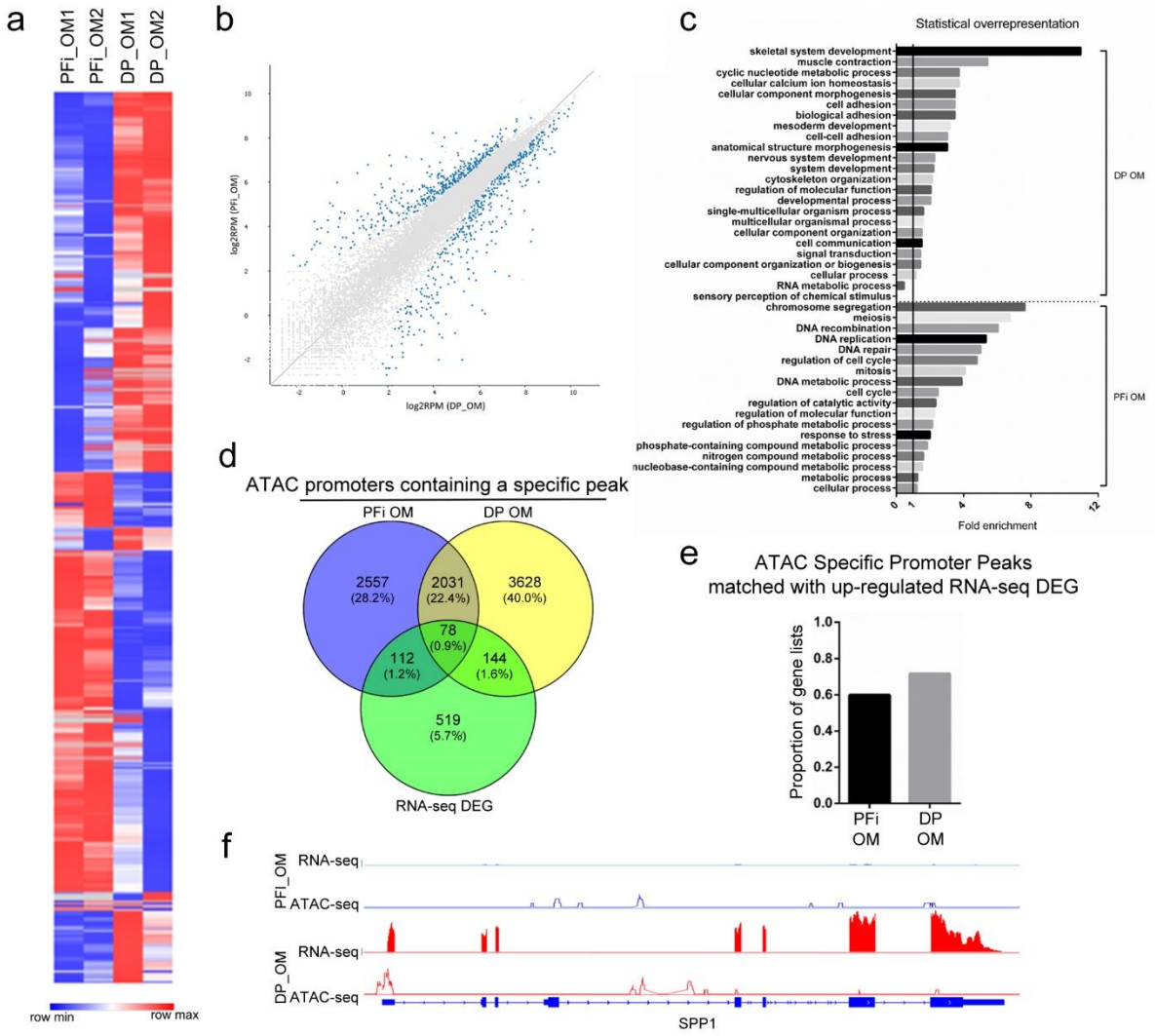

Figure 4. OM Comparison of RNA-seq reveals overrepresentation on skeletal differentiation terms in DP; a) Heat map displaying differentially expressed genes from RNA-seq analysis; b) Scatter plot showing distribution of RNA-seq differentially expressed genes (blue); c) Gene ontology showing statistically over/under-represented biological processes from upregulated genes in each cell type; d) Venn displaying correlation of ATAC promoters and RNA-seq differentially expressed genes; e) Proportion of ATAC promoters that match with upregulated expression in RNA-seq data; f) Example of RNA-seq differentially expressed gene matched with identification of an ATAC specific peak within its promoters. Gene shown*: SPP1.*

and bone marrow mesenchymal stem cells derived from *Spp1*-/- mice demonstrate impaired bone formation both *in vitro* and *in vivo* [19]. As PFi cells do not mineralise in OM, this effect could possibly be driven by inaccessible chromatin around the *SPP1* TSS, leading to an inability of upstream transcription factors to bind and activate gene transcription.

Analysis of the ATAC-seq data of both PFi and DP in OM demonstrated that the fibroblast subtypes have unique chromatin accessibility profiles around TSS, which following ontology analysis revealed the emergence of two distinct epigenetic landscapes. However, neither DP nor PFi in OM, demonstrated a clear enrichment towards a pro- or anti-osteogenic cell phenotype, inferring that chromatin reorganisation may not be driving osteogenic differentiation of DP cells in OM. Comparatively, ontology analysis of the RNA-seq data revealed a prominent overrepresentation of the GO term 'skeletal system development' in DP cells, suggesting that the transcriptional profile of DP cells in OM is highly osteogenic compared to PFi. This suggests a cell specific transcriptional response may be occurring in cells in response to perturbation by OM.

Cell specific epigenetic landscapes arise in PFi and DP cells exposed to OMSW

When fibroblast subtypes were grown in OM, we observed the emergence of an RNA transcriptome in DP cells, with an osteogenic signature. However, the ATAC-seq profiling did not reveal any changes in chromatin indicating an epigenetic response of cells to the OM. We have previously shown that application of a single 165 kPa SW results in a synergistic acceleration and enhancement of mineralisation in DP cells in OM, yet has no effect on PFi [13]. We therefore decided to investigate whether these two perturbing stimuli (a SW together with OM) might result in chromatin reorganisation in a cell specific manner.

To evaluate this, DP and PFi cells were exposed to a single 165 kPa SW using a custom built shock tube [20]. Immediately after this, OM was added to the cells and 24 hours later, DNA and RNA were isolated to generate ATAC and RNA-seq libraries. As before, ATAC libraries showed clear banding patterns (Fig. 5a, Fig. S1), the number of called peaks was well distributed between biological

replicates (Fig. 5b) and FRiP scores were higher than 0.3 (Fig. 5c). Concordance between replicates was 0.9 and 0.93 for PFi OMSW and DP OMSW (Fig. 5d) respectively, and sets were merged for further analysis. The same comparative analysis was performed as in GM and OM to identify condition specific peaks, identifying 215042 shared peaks, 208723 peaks unique to PFi OMSW and 171529 peaks unique to DP OMSW (Fig. 5e). Of these, 8.3% and 8.5% fell within a promoter region in PFi and DP cells (Fig. 5f), respectively. A Venn analysis of this data revealed 3670 unique gene promoters with a condition specific peak in PFi, and 2638 in DP (Fig. 5g). Ontology of these gene lists, described as chromatin accessibility profiles, was performed to identify 5 top physiological system development and functions for PFi and DP in OMSW. In contrast to the GM ontology analysis, which showed a high amount of overlap between PFi and DP in GM (Fig. 1h), exposure to two perturbing stimuli in the form of OMSW appears to generate distinct and unique ontology signatures, with no overlap between DP and PFi cells (Fig. 5h).

To determine if the combination of OM together with a SW also resulted in distinct transcriptional signatures, we performed RNA-seq analysis, identifying 290 and 260 genes significantly upregulated respectively in DP and PFi cells in OMSW (Fig. 6a,b). Ontology analysis of these genes using an overrepresentation test in Panther [17], revealed 4 overrepresented terms in PFi, and 22 in DP (Fig. 6c). In PFi OMSW, all 4 of the overrepresented terms were also identified in the PFi OM ontology analysis (Fig. 6c), suggesting that the SW has little effect on transcriptional activity in PFi. In the DP OMSW analysis 8 of the 22 terms, including ‘cell proliferation’ and ‘cell differentiation’, were new to this analysis compared to the DP OM. Upon exploration of the genes associated found within the ‘cell differentiation’ ontology term, we found transforming growth factor β2 (*TGFβ2*) and *TGFβ3*, genes with known roles in osteogenic differentiation [21].

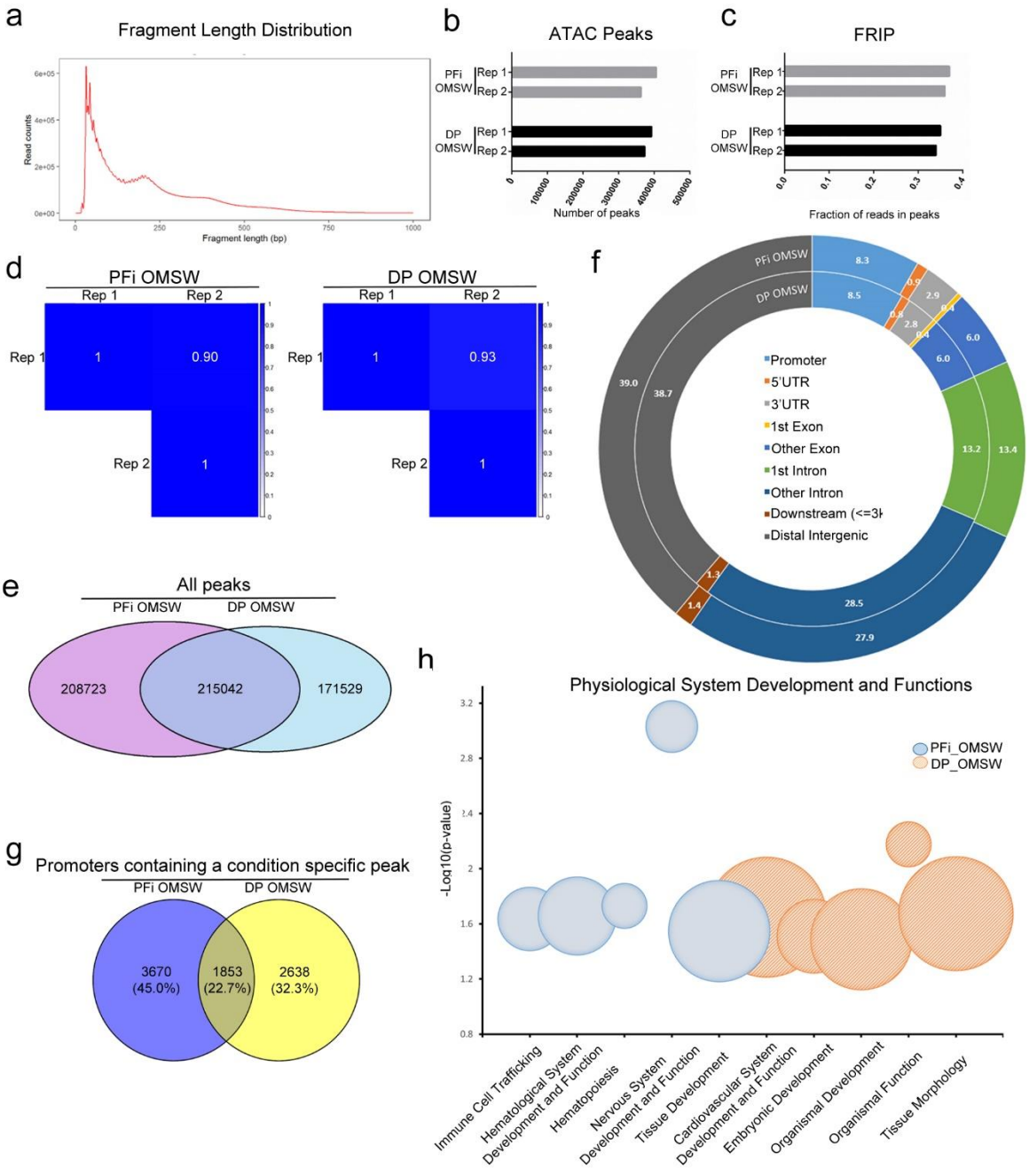

Figure 5. OMSW Comparison uncovers unique chromatin signatures in fibroblasts; a) ATAC-seq nucleosome banding on PFi OMSW library; b) Number of ATAC peaks in individual biological replicates; c) FRiP scores from individual biological replicates; d) Correlation matrix; e) Venn diagram displaying crossover of all ATAC peaks in each condition; f) Peak annotation of specific ATAC peaks on merged samples; g) Venn diagram displaying gene promoters in each condition; h) Gene ontology analysis on ATAC data generated using IPA core analyses. The size of the bubble represents the number of molecules associated within that function.

As in previous comparisons, we also wanted to correlate our chromatin accessibility profile lists and our RNA-seq differentially expressed gene lists, to see if chromatin rearrangements in promoters were affecting transcription. Venn analysis demonstrated some crossover between the two data sets, with 221 out of 550 genes showing overlap (Fig. 6d). Of these, similar rates of directional transcription were observed, with 64% and 71% of genes in PFi and DP OMSW (Fig. 6e) respectively, showing enhanced transcriptional activity with the presence of a condition specific peak located within the promoter region of the target gene, as shown in the example, actin alpha 2 smooth muscle (*ACTA2,* Fig. 6f).

Using ATAC and RNA-seq, we found that DP and PFi exposed to OMSW resulted in the formation of two distinct epigenetic landscapes, containing unique cell specific chromatin accessibility profiles. Overrepresentation analysis of the upregulated genes in PFi OMSW, showed no evidence of differentiation terms, whilst genes in DP OMSW were overrepresented for 'cell differentiation' (Fig. 6c). Assessing the correlation between condition specific ATAC-seq promoters and RNA-seq gene lists we found that a sizable proportion of differentially expressed genes are partially regulated by increased promoter accessibility. The remaining differentially expressed genes are likely regulated

by changes in chromatin accessibility outside of promoter regions. .

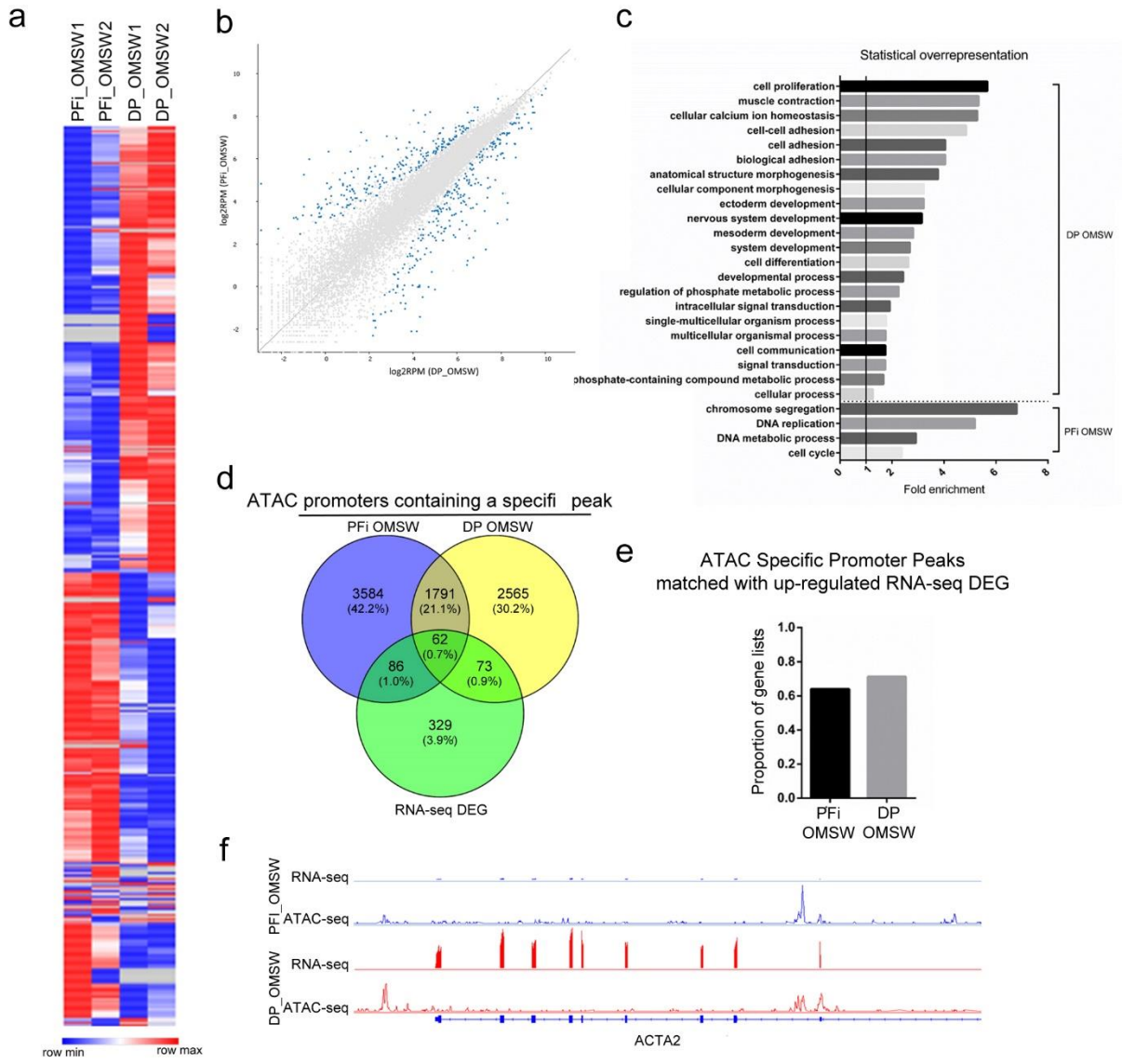

Figure 6. OMSW Comparison uncovers unique chromatin signatures in fibroblasts; a) Heat map displaying differentially expressed genes from RNA-seq analysis; b) Scatter plot showing distribution of RNA-seq differentially expressed genes (blue); c) Gene ontology showing statistically over/under-represented biological processes from upregulated genes in each cell type; d) Venn displaying correlation of ATAC promoters and RNA-seq differentially expressed genes; e) Proportion of ATAC promoters that match with upregulated expression in RNA-seq data; f) Example of RNA-seq differentially expressed gene matched with identification of an ATAC specific peak within its promoters. Gene shown: *ACTA2*.

Multi-way comparative analysis of chromatin organisation reveals DP OMSW are enriched towards an osteogenic identity

Our previous analysis of the ATAC-seq data was designed to identify cell specific changes in chromatin accessibility, as DP and PFi were compared to one another in similar conditions (either GM, OM or OMSW). However, this analysis did not give us insight into the chromatin rearrangements which occur within a cell type as a result of a specific perturbation. Instead, in our inter-cell comparisons of chromatin accessibility we identified lists of genes that contained a condition specific peak within their promoter region unique to the cell type in that comparison. To narrow our focus, and acquire lists that contained genes unique to both a cell type and a specific perturbation, we evaluated these inter-cell comparison lists by performing a 6 way Venn [22]. Visualisation of the Venn analysis using intersection analysis [23] showed that whilst some genes were shared between cell types and across comparisons, the largest groups of genes were ones unique to a single cell type and condition (Fig. 7a).

When we initiated this work, we postulated that cell specific epigenetic differences were enabling DP cells, but not PFi to mineralise *in vitro* when cultured in OM. As SW exposure could enhance mineralisation [13], we specifically wanted to analyse the effect of a SW on DP chromatin organisation. Using the unique lists exported from our 6 way Venn analysis, we performed IPA ontology of the genes found only within DP cells in the OMSW comparison, identifying multiple networks strongly associated with osteogenic functions (Fig. 7b). The top network generated in core analysis from IPA in DP OMSW showed interactions of our identified genes with a number of osteogenic master regulators, such as Runt-related transcription factor 2 (*RUNX2*) [24] and Osterix (*SP7*) [25] (Fig. 7c). Notably, inclusion and predicted activation of integrin alpha V (*ITGAV*) was also observed within the network (Fig. 7c). ITGAV is a cell surface mechanosensor, which increases in expression in mesenchymal stem cells undergoing osteogenic differentiation [26] , while knockdown can lead to adipogenic differentiation in adipose stem cells [27]. We previously identified *ITGAV* as a

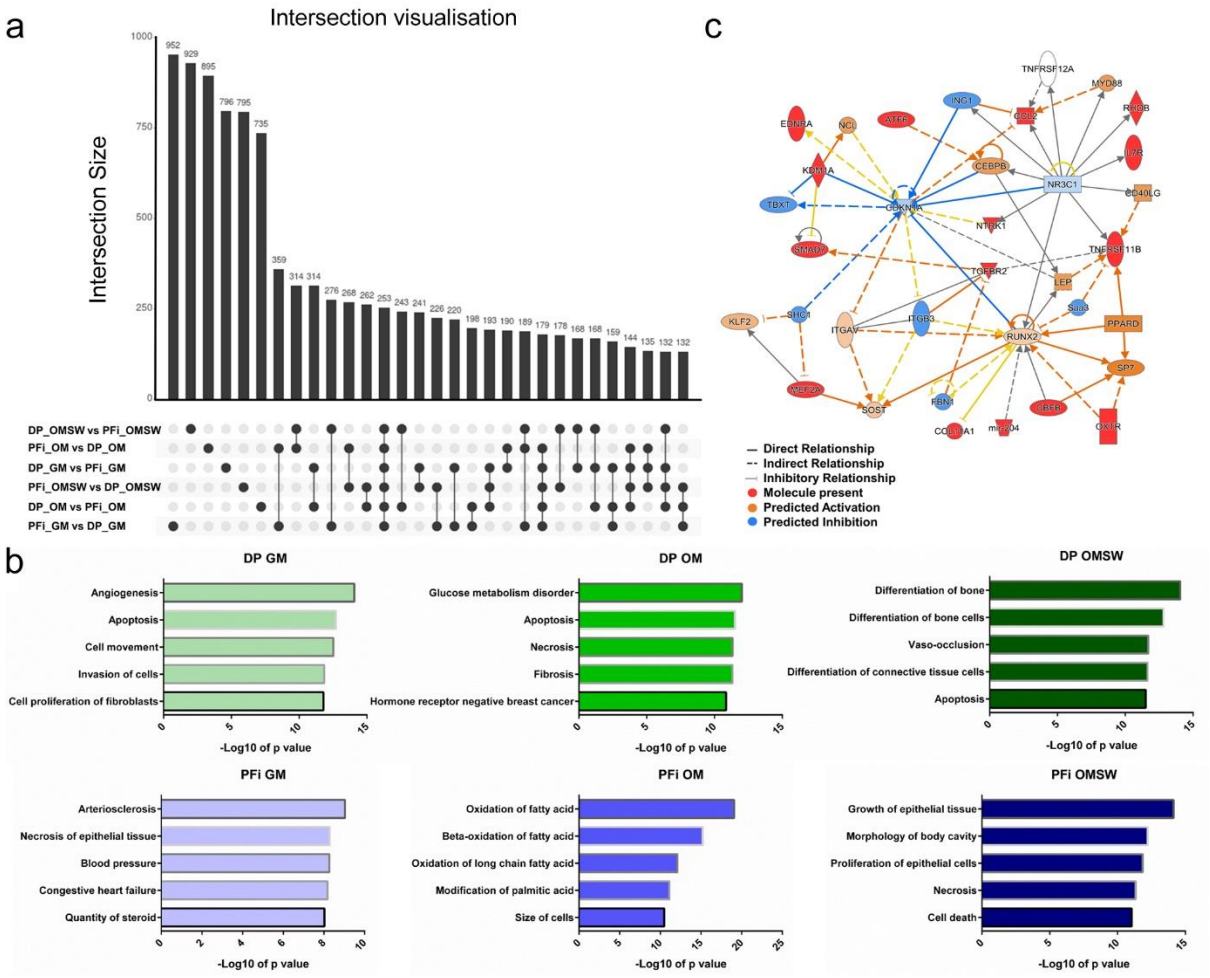

Figure 7. Comparative analysis shows osteogenic enrichment in DP OMSW chromatin profile; a) Intersection visualisation analysis showing the presence of a high number of unique genes in each cell type within each comparison; b) IPA generated network from the unique DP OMSW gene list taken from intersection analysis, showing osteogenic associated interactions; c) Comparison of the top 5 functions associated with the top generated IPA network created using intersection analysis unique gene lists. Only DP OMSW was found to possess osteogenic associated chromatin networks.

biomarker of OMSW-induced ectopic mineralisation, and demonstrated that ITGAV inhibition can abrogate OMSW induced mineral deposition in DP cells *in vitro* [13]. The inclusion and predicted activation of *ITGAV* within the top pathway analysis network generated from chromatin accessible unique DP OMSW genes, strengthens our hypothesis that *ITGAV* is a key component in OMSW-

induced ossification. To assess if the incorporation of *ITGAV* and other osteogenic associated genes into the top networks generated in IPA was specific, or an artefact of IPA, we also assessed the top networks generated in IPA from the other five unique gene lists from our 6 way Venn analysis. We found that no other gene lists, including the DP OM list, resulted in generation of IPA networks containing a single osteogenic associated function (Fig. 7b). This data implies that within the OMSW comparison, DP cells have unique chromatin accessibility at gene promoters enabling enhanced osteogenic differentiation. Considering the absence of osteogenic associated networks generated from chromatin accessibility lists from DP OM, which do ossify albeit slower than DP OMSW, our analysis suggests that restructuring of chromatin occurs as a result of SW exposure in a cell specific manner. We propose that this leads to the formation of an epigenetic landscape enriched towards osteogenic differentiation and helps to explain the accelerated ossification observed in DP cells in response to SW exposure.

Discussion

In this body of work, we wanted to understand why two sister cell types, which arise from a common progenitor during development [9], have different potential for osteogenic differentiation *in vitro* [13]. We hypothesised that baseline differences in the epigenetic status of these two fibroblast subtypes, DP and PFi, were enabling this differential response. However, using ATAC-seq to evaluate regions of open chromatin, we found that the chromatin accessibility profile of both DP and PFi in GM results in activation of genes with comparable ontological networks, suggesting inherent similarities in the chromatin architecture between the cell types. When perturbing stimuli which enhance ossification of DP cells, but not PFi, were introduced, we gradually observed a divergence of the epigenetic signatures of the fibroblast subtypes, suggesting that the stimuli itself elicit a cell specific response. Specifically, we found that when DP cells are exposed to both mechanical stimulation (a SW), and chemical stimulation (OM), which we know can enhance and accelerate ossification of DP cells [13], they acquire a unique chromatin profile of accessible

promoters at genes associated with osteogenic differentiation (Fig. 7bc). As samples were analysed just 24 hours after exposure to OMSW, several days before osteogenic differentiation actually occurs, it suggests these chromatin rearrangements occur as a result of exposure to stimuli, which leads to differentiation, rather than occurring as a result of differentiation. This makes it even more intriguing that PFi do not show the same rearrangements, highlighting that we are observing not only a differential ability of DP and PFi to ossify, but a cell specific chromatin rearrangement response to mechanical and chemical perturbations.

The effect of chromatin accessibility on cell differentiation is now beginning to be investigated fully and reported in the literature thanks to recent advances in genomic sequencing technologies. Using DNAse 1 hypersensitivity to assess a human fetal osteoblastic cell line (hFOB) *Thompson et al* detected large scale reorganisation of the chromatin landscape upon osteogenic induction, with clear changes present between cells in basal media or OM after 48 hours of differentiation [28]. As in the present study, promoter regions were assessed and significant changes in chromatin accessibility were also present. To identify potential transcription factors that may be binding promoters and affecting the differentiation of hFOBs, motif analysis was performed and revealed that cells in OM had accessible chromatin at binding motifs for the osteogenic master regulator RUNX2 [28].

In DP cells exposed to perturbation with OMSW, we identified changes occurring to the chromatin epigenetic landscape which were associated with enhancement of ossification. It has previously been proposed that application of mechanical forces can lead to both short-term and long-term changes to chromatin function. Short-term responses, described as a mechano-response, can lead to chromatin decondensation at force-selective genes that could be a means to dissipate mechanical stress [29]. It is thought that outside-in signalling via cell surface integrins can propagate stresses to the actin cytoskeleton, resulting in changes to nuclear lamins and subsequently chromatin decondensation [30]. How these mechanical stresses are transferred from nuclear lamins to

chromatin is likely affected by chromosomal locations within the nucleus [31], and this positioning may explain cell specific responses to mechanical forces. Effects from long duration mechanical forces, described as mechano-adaption [29], can lead to chromatin compaction [32], highlighting the ability as well as the complexity of the effect of mechanical stimulation on cell response.

Here, we observed that a mechanical stimulus, in the form of a SW, could result in changes in chromatin accessibility in a cell specific manner, leading to enhanced osteogenic differentiation. We have previously shown that another epigenetic mechanism, DNA methylation, is also altered in DP and human bone marrow mesenchymal stem cells, in OMSW [13]. One of the genes whose promotor was hypo-methylated as a result of SW exposure in OM was the osteogenic associated [26] mechano-sensor *ITGAV*, which was also identified as activated within the top chromatin accessibility network from DP cells in OMSW in this current study (Fig. 7b). Expression of *ITGAV* is also significantly increased in DP OMSW mRNA verses PFi cells in OMSW (Fig. 6a,b), which notably are unable to mineralise. In summary, we have demonstrated both changes to chromatin accessibility (Fig. 7bc) and DNA methylation [13] of *ITGAV* and other genes, which occur in a cell specific manner in response to perturbation with OMSW, resulting in enhanced ossification *in vitro*.

To conclude, in this body of work we used ATAC-seq combined with RNA-seq, to demonstrate that exposure to a mechanical stimulus (SW) together with a chemical stimulus (OM) elicits a cell specific response in human DP cells, modifying chromatin accessibility and enabling accelerated differentiation down an osteogenic lineage.

Materials and methods

Study design

Here, we performed a combination of ATAC-seq and RNA-seq on human DP and PFi cells cultured in growth (GM) or osteogenic media (OM) only, or osteogenic media plus exposure to a shock wave (OMSW). The main aim of this was to assess the role of chromatin structure in osteogenic

differentiation, and determine if certain cell types are sensitised to differentiation down an osteogenic linage. We performed our experiments in three stages: (i) Firstly we gathered DNA and RNA for sequencing from both DP and PFi cells, in the following conditions; GM, OM and OM plus a 165kPa SW (OMSW); (ii) using both the DNA and RNA gathered in step (i) we performed ATAC library preparation for sequencing following a previously published protocol [14, 33], and RNA-seq using Smart-seq2 library preparation [34]; (iii) we then completed bioinformatics analysis on ATAC libraries using an esATAC R script, and RNA libraries with SeqMonk. Three inter-cell comparative analyses were performed, first by comparing PFi and DP in GM, followed by PFi and DP in OM, and lastly PFi and DP in OMSW comparison. We generated lists containing differentially expressed genes or condition specific ATAC peaks, and analysed downstream functions controlled by these genes in IPA. Differentially expressed genes generated from RNA-seq data was validated using RT-qPCR; (iv) lastly, we performed comparative analysis between our ATAC lists from each comparison using UpSet and InteractiVenn, revealing the relationship between chromatin structure and how it can sensitise cells towards an osteogenic identity. The sample sizes for our *in vitro* tests were taken from similar studies reported in the literature. The exact number for each experiment can be found in the figure legends. Investigators were not blinded when conducting or evaluating the experiments.

Cell isolation and culture

DP and PFi cells were isolated from discarded tissue from patients undergoing hair transplant surgeries after written informed consent was obtained. Microdissection techniques were used to isolate both DP and PFi from the tissue as previously described [35]. Cells were cultured in GM, that consisted of DMEM (ThermoFisher, 61965-026) supplemented with 10% FBS and 1% penicillin/streptomycin (P/S, Thermofisher, 15070-063). OM consisted of low glucose DMEM (LG-DMEM, Thermofisher, 31885-023) containing 10% FBS, 1% P/S, 100 nM dexamethasone (Sigma Aldrich, D4902), 50 µM L-ascorbic acid 2-phosphate (Sigma Aldrich, A8960) and 10 mM β-glycerol phosphate (Sigma Aldrich, G9422).

469 *Shock wave exposure*

470 DP and PFi cells were seeded into 35mm petri dishes at 7 x 10^4 cells per dish and left overnight in
471 standard culture conditions of 37°C, 5% CO_2 in a humidified environment. The following day, using a
472 compressed air-driven shock tube, cells were exposed to one 165kPa shock wave as previously
473 described [13, 20]. Medium was changed to either GM or OM immediately following shock wave
474 exposure. 24 hr post shock wave exposure, cells were harvested to be used for DNA or RNA
475 isolation.

476 *RNA-seq*

477 DP and PFi cells in GM, OM and OMSW were homogenized by centrifugation through Qiashredders
478 (Qiagen, 79654), and total RNA was isolated using a commercially available kit as per the
479 manufacturer's instructions (Qiagen, RNeasy Plus Micro kit, 74034). Quality control was performed
480 in the form of a Qubit RNA high sensitivity assay (ThermoFisher, Q32852), NanoDrop
481 Spectrophotometry and Agilent Technologies Bioanalyzer to attain RNA integrity (RIN) scores. All
482 samples had RIN numbers >9. cDNA library construction was performed at Oxford Genomics
483 (Oxford, United Kingdom) using the Smart-seq2 library preparation protocol [34] and libraries were
484 sequenced using 75bp paired-end-reads on 2 lanes of an Illunmia HiSeq 4000 instrument. Samples
485 were re-pooled when running the second lane to generate libraries of approximately equal size.

486 *ATAC-seq*

487 Libraries for ATAC-seq were generated by following a previously reported method [14, 33]. Cells
488 were washed twice in ice-cold PBS and incubated with 0.5% trypsin-EDTA for 5 minutes until the
489 cells dissociated from the dish. Media was then added to the cells, which were centrifuged at 300g
490 for 4 minutes to form a pellet. The pellet was re-suspended in fresh media, counted, and the
491 volume of media adjusted to attain a 4.5 x 10^4 cells/ml concentration. 1 ml of each suspension was
492 then transferred to a 1.5 ml Eppendorf tube, centrifuged at 500g for 5 minutes at 4°C, and re-

493 suspended in 50µl of ice-cold PBS. Following a further centrifugation under the same conditions, the
494 pellet was re-suspended in 50µl of a transposition mix containing TD Buffer (25µl), TDE1 (2.5µl),
495 nuclease free water (22µl) and digitonin 1% (0.5µl)(Illumina FC-121-1030). Samples were incubated
496 with the transposition mix for 30 minutes, undergoing a brief vortex every 10 minutes. Immediately
497 after incubation, transposed samples were purified using the MinElute PCR Purification kit (Qiagen,
498 28004) as per the manufacturer's instructions and PCR amplified with Nextera sequencing adaptors
499 for 11-13 cycles. Right side size SPRI bead selection with a ratio of x0.5 was then performed to
500 remove fragments under 100bp and over 1000bp in size (Beckman, B23317). Quality control was
501 performed using Qubit High Sensitivity DNA assay (ThermoFisher Q32851) and Agilent Technologies
502 Bioanalyzer, to check for nucleosome banding within the generated libraries. Libraries were
503 sequenced using 75bp paired-end-reads on 2 lanes of an Illumina HiSeq 4000 instrument.

504 *RNA-seq data analysis*

505 Sequenced reads were assessed for quality using FastQC [36] and trimmed of overrepresented
506 sequences and adapter contamination from the Smart-Seq2 library preparation. Post trimming
507 reads were then aligned to the human genome (hg19) using the HISAT2 aligner with default
508 parameters [37]. The generated SAM files were converted to BAMs using SAMtools [38], and
509 matched BAM files from both lanes were merged using Picard. Merged BAMS were assessed within
510 SeqMonk using the RNA-seq quantitation pipeline. Within the SeqMonk graphical user interface,
511 DESeq2 was used to identify differentially expressed genes, using multiple correction testing (FDR
512 ≤0.01) and a p-value cut-off of ≤0.05 [39]. Heat-maps of differentially expressed genes were
513 generated using Morpheus using the one minus pearson correlation for hierarchical clustering.
514 Ontology of up-regulated genes in each cell type was performed using the statistical
515 overrepresentation test in Panther on default settings including an FDR test correction [17].

516 *ATAC-seq data analysis*

Sequenced raw reads in FastQ format from lane 1 and 2 were merged and processed using the esATAC R script, an all-in-one ATAC-seq analysis pipeline [40]. Within the esATAC pipeline, AdapterRemoval [41] was used for adapter trimming and alignment to the human genome (hg19) was performed using Bowtie2 with ATAC-seq bespoke parameters [42]. Sorting of reads, duplicate removal and read shifting due to Tn5 insertion were performed within the esATAC pipeline. The identification of open chromatin peaks was performed using F-seq [43] followed by peak annotation using ChIPseeker [44]. Within the esATAC pipeline, comparative analysis between the cell types in each condition was then performed to identify condition specific peaks. A condition specific peak can be defined as a peak that has been called in one cell type that is not present in the exact matching genomic location in other cell types within the comparison. The annotated lists containing all of the condition specific peak locations were then filtered for gene promoters (esATAC default settings of +/- 3000bp around the transcription start site). Any gene that contained a condition specific peak within its promoter range in both cell types of interest were discarded. Using the remaining genes that contained a condition specific peak within their promoters, gene ontology was performed using Ingenuity Pathway Analysis (IPA, QIAGEN Inc). The top 5 physiological system development and functions for each condition, generated through a core analysis, were reported as a bubble graph with the size of the bubble representative of the number of genes for that category. Lastly, crossover analysis between RNA-seq differentially expressed genes and ATAC gene promoters was performed. Integrative Genomics Viewer was used to view sequenced data-sets [45, 46].

ATAC-seq comparative analysis

The ATAC-seq promoter gene lists from each comparison, inclusive of gene promoters that contained a condition specific peak in both cell types were compared and visualised using UpSet [23] to assess variation in chromatin peaks across all the conditions and cell types. Using the InteractiVenn online tool [22] and same datasets used in UpSet intersection visualisation, gene lists containing comparison unique genes were exported and assessed in IPA using core analysis.

mRNA validation

Reverse transcriptase quantitative polymerase chain reaction (RT-qPCR) was performed to validate RNA-seq pipeline analysis. Glyceraldehyde-3-phosphate dehydrogenase (GAPDH) was used as the housekeeping control. SW exposed cells were harvested for RNA isolation. The cells were homogenized by centrifugation through Qiashredders, and RNA was isolated using a commercially available kit as per the manufacturer's instructions (Qiagen, RNeasy Plus Micro kit, 74034). A total of 100ng of isolated RNA was then synthesised into complimentary DNA by reverse transcription (cDNA, SuperScript III Reverse Transcriptase, ThermoFisher, 18080-093). To quantify mRNA expression, quantitative PCR was performed using a StepOnePlus system (Applied Biosystems). cDNA was combined together with H_2O and Syber reagents (PowerUp Syber Green Master Mix, ThermoFisher, A25779). RT-qPCR reactions were performed in quadruplicate. The thermocyclic conditions included an initial hold stage of 50°C for 2 min then 95°C for 2 minutes, followed by 40 cycles of 95°C for 15 sec and 60°C for 1 min. Results were normalised to GAPDH and calculated using the ΔΔCt method. Statistical analyses were performed in GraphPad Prism (Version 6). Statistical differences were assessed using a two tailed Student's t test. A p-value of ≤0.05 was deemed to be statistically significant. Validated RT-qPCR genes from RNA-seq pipeline analyses are shown in Fig. S2. The GAPDH primer was taken from [47] while other primers were designed against sequences in the UCSC database (Table S1).

List of Abbreviations

OM: Osteogenic Media

GM: Growth Media

OMSW: Osteogenic Media + Shock Wave

SW: Shock Wave

DP: Dermal Papilla

PFi: Papillary Fibroblasts

ATAC-seq: Assay for transposase accessible chromatin in combination with high throughput sequencing

RNA-seq: RNA-sequencing

IPA: Ingenuity Pathway Analysis

Declarations

- *Ethics approval and consent to participate*

DP and PFi were isolated from human tissues, collected from patients who gave their written informed consent using Joint Research Compliance Office approved consent forms (Imperial College Research Ethics Committee reference: 17IC3726). Tissue was held in the Imperial College Healthcare Tissue Bank (ICHTB) under the Human Tissue Authority license 12275 and used in the ICHTB approved project R15055-1A. The study itself, and experimental protocols associated with the study, were approved by the Joint Research Compliance Office. Methods were performed in accordance with the relevant guidelines and regulations.

- *Consent for publication*

Not applicable: there are no details, images or video's relating to an individual person in this manuscript.

- *Availability of data and materials*

Both ATAC-seq (SRA: SRP192978, https://trace.ncbi.nlm.nih.gov/Traces/sra/?study=SRP192978) and RNA-seq (SRA: SRP287348, https://trace.ncbi.nlm.nih.gov/Traces/sra/sra.cgi?study=SRP287348) raw data are available on the NCBI Sequencing Read Archive.

- *Competing interests*

The authors declare they have no competing interests.

- *Funding*

590 This project was funded with a grant from the Medical Research Council (M01858X/1) to CAH
591 (https://mrc.ukri.org/). The funders had no role in study design, data collection and analysis,
592 decision to publish, or preparation of the manuscript.

593 • *Authors' contributions*

594 NJL performed the laboratory work, devised experimental plans and wrote the paper. CAH designed
595 the project and co-wrote the manuscript. NP provided bioinformatics analysis support and
596 performed laboratory work. MC performed laboratory work. GW consented patients and provided
597 tissue samples. All authors read and approved the manuscript.

598 • *Acknowledgements*

599 We would like to acknowledge support from the Centre for Blast Injury Studies (Imperial College
600 London), for giving us access to their bespoke shock tube.

601 **References**

602 1. Tsompana M, Buck MJ: Chromatin accessibility: a window into the genome. *Epigenet*
603 *Chromatin* 2014, 7.
604 2. Adam RC, Yang H, Ge Y, Lien WH, Wang P, Zhao Y, Polak L, Levorse J, Baksh SC, Zheng D *et al*:
605 Temporal Layering of Signaling Effectors Drives Chromatin Remodeling during Hair Follicle
606 Stem Cell Lineage Progression. *Cell Stem Cell* 2018, 22(3):398-413 e397.
607 3. Liu Q, Jiang C, Xu J, Zhao M, Van Bortle K, Cheng X, Wang G, Chang HY, Wu JC, Snyder MP:
608 Genome-Wide Temporal Profiling of Transcriptome and Open-Chromatin of Early
609 Cardiomyocyte Differentiation Derived From hiPSCs and hESCs. *Circulation Research* 2017.
610 4. Nelson AC, Mould AW, Bikoff EK, Robertson EJ: Mapping the chromatin landscape and
611 Blimp1 transcriptional targets that regulate trophoblast differentiation. *Sci Rep-Uk* 2017, 7.
612 5. Guo J, Grow EJ, Yi C, Mlcochova H, Maher GJ, Lindskog C, Murphy PJ, Wike CL, Carrell DT,
613 Goriely A *et al*: Chromatin and Single-Cell RNA-Seq Profiling Reveal Dynamic Signaling and

Metabolic Transitions during Human Spermatogonial Stem Cell Development. *Cell Stem Cell* 2017, 21(4):533-546.e536.

6. Daugherty AC, Yeo RW, Buenrostro JD, Greenleaf WJ, Kundaje A, Brunet A: Chromatin accessibility dynamics reveal novel functional enhancers in C. elegans. *Genome Res* 2017, 27(12):2096-2107.

7. Ackermann AM, Wang Z, Schug J, Naji A, Kaestner KH: Integration of ATAC-seq and RNA-seq identifies human alpha cell and beta cell signature genes. *Molecular Metabolism* 2016, 5(3):233-244.

8. Philippeos C, Telerman SB, Oules B, Pisco AO, Shaw TJ, Elgueta R, Lombardi G, Driskell RR, Soldin M, Lynch MD *et al*: Spatial and Single-Cell Transcriptional Profiling Identifies Functionally Distinct Human Dermal Fibroblast Subpopulations. *J Invest Dermatol* 2018, 138(4):811-825.

9. Driskell RR, Lichtenberger BM, Hoste E, Kretzschmar K, Simons BD, Charalambous M, Ferron SR, Herault Y, Pavlovic G, Ferguson-Smith AC *et al*: Distinct fibroblast lineages determine dermal architecture in skin development and repair. *Nature* 2013, 504(7479):277-281.

10. Myllylä RM, Haapasaari K-M, Lehenkari P, Tuukkanen J: Bone morphogenetic proteins 4 and 2/7 induce osteogenic differentiation of mouse skin derived fibroblast and dermal papilla cells. *Cell and Tissue Research* 2014, 355(2):463-470.

11. Jahoda CAB, Whitehouse CJ, Reynolds AJ, Hole N: Hair follicle dermal cells differentiate into adipogenic and osteogenic lineages. *Experimental Dermatology* 2003, 12(6):849-859.

12. Richardson GD, Arnott EC, Jenna Whitehouse C, Lawrence CM, Hole N, Jahoda CAB: Cultured Cells from the Adult Human Hair Follicle Dermis can be Directed Toward Adipogenic and Osteogenic Differentiation. *Journal of Investigative Dermatology* 2005, 124(5):1090-1091.

13. Logan NJ, Camman M, Williams G, Higgins CA: Demethylation of ITGAV accelerates osteogenic differentiation in a blast-induced heterotopic ossification in vitro cell culture model. *Bone* 2018, 117:149-160.

14. Buenrostro JD, Wu B, Chang HY, Greenleaf WJ: ATAC-seq: A Method for Assaying Chromatin Accessibility Genome-Wide. *Curr Protoc Mol Biol* 2015, 109:21 29 21-29.

15. Muller F, Tora L: Chromatin and DNA sequences in defining promoters for transcription initiation. *Biochim Biophys Acta* 2014, 1839(3):118-128.

16. Higgins CA, Chen JC, Cerise JE, Jahoda CAB, Christiano AM: Microenvironmental reprogramming by three-dimensional culture enables dermal papilla cells to induce de novo human hair-follicle growth. *Proceedings of the National Academy of Sciences* 2013, 110(49):19679-19688.

17. Thomas PD, Campbell MJ, Kejariwal A, Mi H, Karlak B, Daverman R, Diemer K, Muruganujan A, Narechania A: PANTHER: a library of protein families and subfamilies indexed by function. *Genome Res* 2003, 13(9):2129-2141.

18. Janson DG, Saintigny G, van Adrichem A, Mahe C, El Ghalbzouri A: Different gene expression patterns in human papillary and reticular fibroblasts. *J Invest Dermatol* 2012, 132(11):2565-2572.

19. Chen Q, Shou P, Zhang L, Xu C, Zheng C, Han Y, Li W, Huang Y, Zhang X, Shao C *et al*: An osteopontin-integrin interaction plays a critical role in directing adipogenesis and osteogenesis by mesenchymal stem cells. *Stem Cells* 2014, 32(2):327-337.

20. Logan NJ, Arora H, Higgins CA: Evaluating Primary Blast Effects In Vitro. *J Vis Exp* 2017, 127(127):e55618.

21. Chen G, Deng C, Li YP: TGF-beta and BMP signaling in osteoblast differentiation and bone formation. *Int J Biol Sci* 2012, 8(2):272-288.

22. Heberle H, Meirelles GV, da Silva FR, Telles GP, Minghim R: InteractiVenn: a web-based tool for the analysis of sets through Venn diagrams. *Bmc Bioinformatics* 2015, 16.

23. Lex A, Gehlenborg N, Strobelt H, Vuillemot R, Pfister H: UpSet: Visualization of Intersecting Sets. *IEEE Trans Vis Comput Graph* 2014, 20(12):1983-1992.

24. Xu J, Li Z, Hou Y, Fang W: Potential mechanisms underlying the Runx2 induced osteogenesis of bone marrow mesenchymal stem cells. *American Journal of Translational Research* 2015, 7(12):2527-2535.

25. Nakashima K, Zhou X, Kunkel G, Zhang ZP, Deng JM, Behringer RR, de Crombrugghe B: The novel zinc finger-containing transcription factor Osterix is required for osteoblast differentiation and bone formation. *Cell* 2002, 108(1):17-29.

26. Olivares-Navarrete R, Hyzy SL, Park JH, Dunn GR, Haithcock DA, Wasilewski CE, Boyan BD, Schwartz Z: Mediation of osteogenic differentiation of human mesenchymal stem cells on titanium surfaces by a Wnt-integrin feedback loop. *Biomaterials* 2011, 32(27):6399-6411.

27. Morandi EM, Verstappen R, Zwierzina ME, Geley S, Pierer G, Ploner C: ITGAV and ITGA5 diversely regulate proliferation and adipogenic differentiation of human adipose derived stem cells. *Sci Rep-Uk* 2016, 6:28889.

28. Thompson B, Varticovski L, Baek S, Hager GL: Genome-Wide Chromatin Landscape Transitions Identify Novel Pathways in Early Commitment to Osteoblast Differentiation. *Plos One* 2016, 11(2).

29. Miroshnikova YA, Nava MM, Wickstrom SA: Emerging roles of mechanical forces in chromatin regulation. *Journal of Cell Science* 2017, 130(14):2243-2250.

30. Tajik A, Zhang Y, Wei F, Sun J, Jia Q, Zhou W, Singh R, Khanna N, Belmont AS, Wang N: Transcription upregulation via force-induced direct stretching of chromatin. *Nat Mater* 2016, 15(12):1287-1296.

31. Dixon JR, Gorkin DU, Ren B: Chromatin Domains: The Unit of Chromosome Organization. *Mol Cell* 2016, 62(5):668-680.

32. Le HQ, Ghatak S, Yeung CYC, Tellkamp F, Gunschmann C, Dieterich C, Yeroslaviz A, Habermand B, Pombo A, Niessen CM *et al*: Mechanical regulation of transcription controls Polycomb-mediated gene silencing during lineage commitment. *Nat Cell Biol* 2016, 18(8):864-+.

33. Corces MR, Buenrostro JD, Wu B, Greenside PG, Chan SM, Koenig JL, Snyder MP, Pritchard JK, Kundaje A, Greenleaf WJ *et al*: Lineage-specific and single-cell chromatin accessibility charts human hematopoiesis and leukemia evolution. *Nat Genet* 2016, 48(10):1193-1203.

34. Picelli S, Faridani OR, Bjorklund AK, Winberg G, Sagasser S, Sandberg R: Full-length RNA-seq from single cells using Smart-seq2. *Nat Protoc* 2014, 9(1):171-181.

35. Topouzi H, Logan NJ, Williams G, Higgins CA: Methods for the isolation and 3D culture of dermal papilla cells from human hair follicles. *Exp Dermatol* 2017, 26(6):491-496.

36. FastQC [https://www.bioinformatics.babraham.ac.uk/projects/fastqc/]

37. Kim D, Landmead B, Salzberg SL: HISAT: a fast spliced aligner with low memory requirements. *Nat Methods* 2015, 12(4):357-U121.

38. Li H, Handsaker B, Wysoker A, Fennell T, Ruan J, Homer N, Marth G, Abecasis G, Durbin R, Genome Project Data Processing S: The Sequence Alignment/Map format and SAMtools. *Bioinformatics* 2009, 25(16):2078-2079.

39. Love MI, Huber W, Anders S: Moderated estimation of fold change and dispersion for RNA-seq data with DESeq2. *Genome Biol* 2014, 15(12):550.

40. Wei Z, Zhang W, Fang H, Li Y, Wang X: esATAC: An Easy-to-use Systematic pipeline for ATAC-seq data analysis. *Bioinformatics* 2018.

41. Schubert M, Lindgreen S, Orlando L: AdapterRemoval v2: rapid adapter trimming, identification, and read merging. *BMC Res Notes* 2016, 9:88.

42. Langmead B, Salzberg SL: Fast gapped-read alignment with Bowtie 2. *Nat Methods* 2012, 9(4):357-359.

43. Boyle AP, Guinney J, Crawford GE, Furey TS: F-Seq: a feature density estimator for high-throughput sequence tags. *Bioinformatics* 2008, 24(21):2537-2538.

44. Yu G, Wang LG, He QY: ChIPseeker: an R/Bioconductor package for ChIP peak annotation, comparison and visualization. *Bioinformatics* 2015, 31(14):2382-2383.

45. Robinson JT, Thorvaldsdottir H, Winckler W, Guttman M, Lander ES, Getz G, Mesirov JP: Integrative genomics viewer. *Nat Biotechnol* 2011, 29(1):24-26.

46. Thorvaldsdottir H, Robinson JT, Mesirov JP: Integrative Genomics Viewer (IGV): high-performance genomics data visualization and exploration. *Brief Bioinform* 2013, 14(2):178-192.

47. Farshdousti Hagh M, Noruzinia M, Mortazavi Y, Soleimani M, Kaviani S, Abroun S, Dehghani Fard A, Mahmoodinia M: Different Methylation Patterns of RUNX2, OSX, DLX5 and BSP in Osteoblastic Differentiation of Mesenchymal Stem Cells. *Cell J* 2015, 17(1):71-82.

Figures

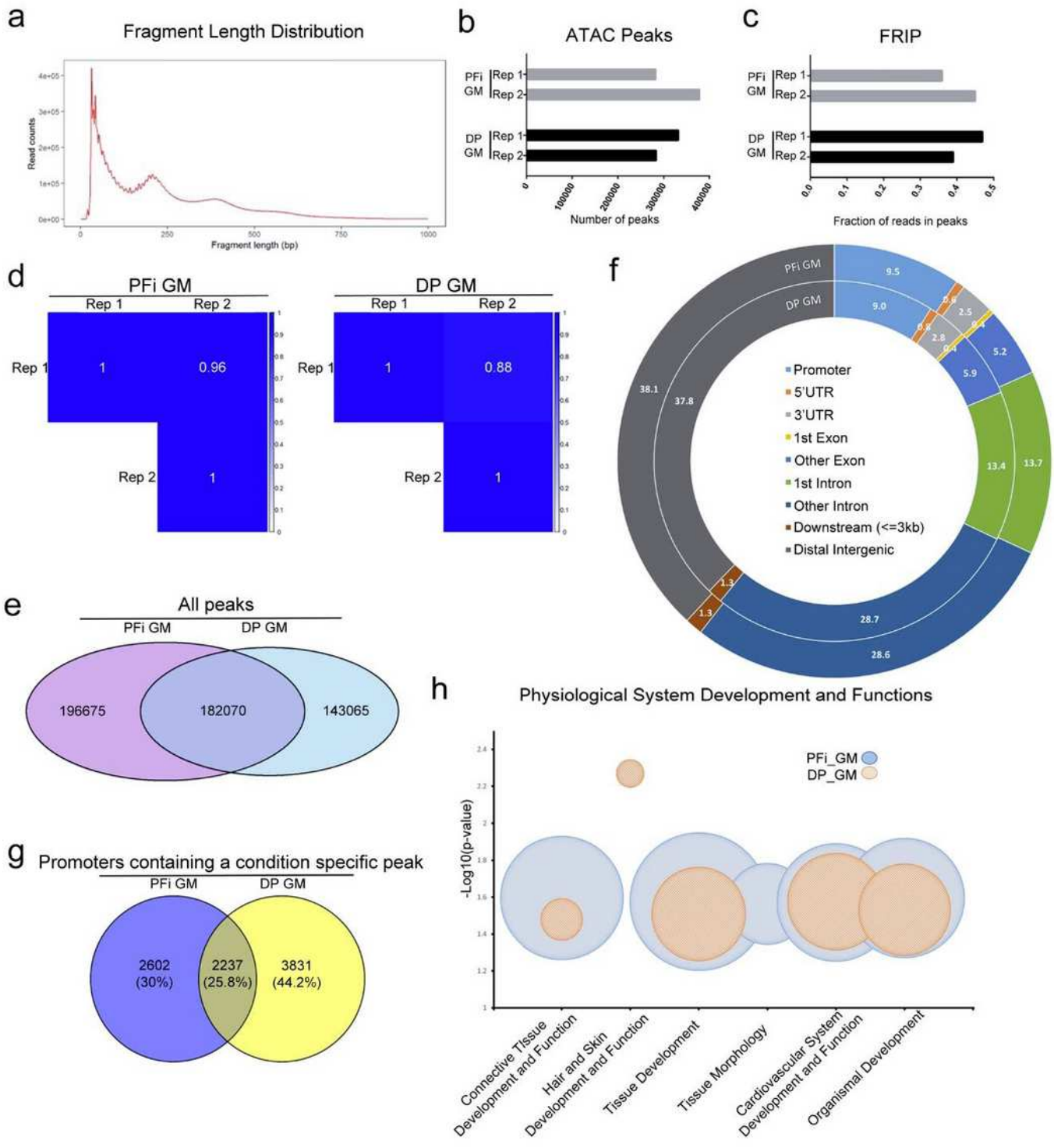

Figure 1

GM Comparison of ATAC-seq data shows similarities between fibroblast subtypes; a) ATAC-seq nucleosome banding on PFi GM library; b) Number of ATAC peaks in individual biological replicates; c) FRiP scores from individual biological replicates; d) Correlation matrix; e) Venn diagram displaying

crossover of all ATAC peaks in each condition; f) Peak annotation of specific ATAC peaks on merged samples; g) Venn diagram displaying gene promoters in each condition; h) Gene ontology analysis on ATAC data generated using IPA core analyses. The size of the bubble represents the number of molecules associated within that function.

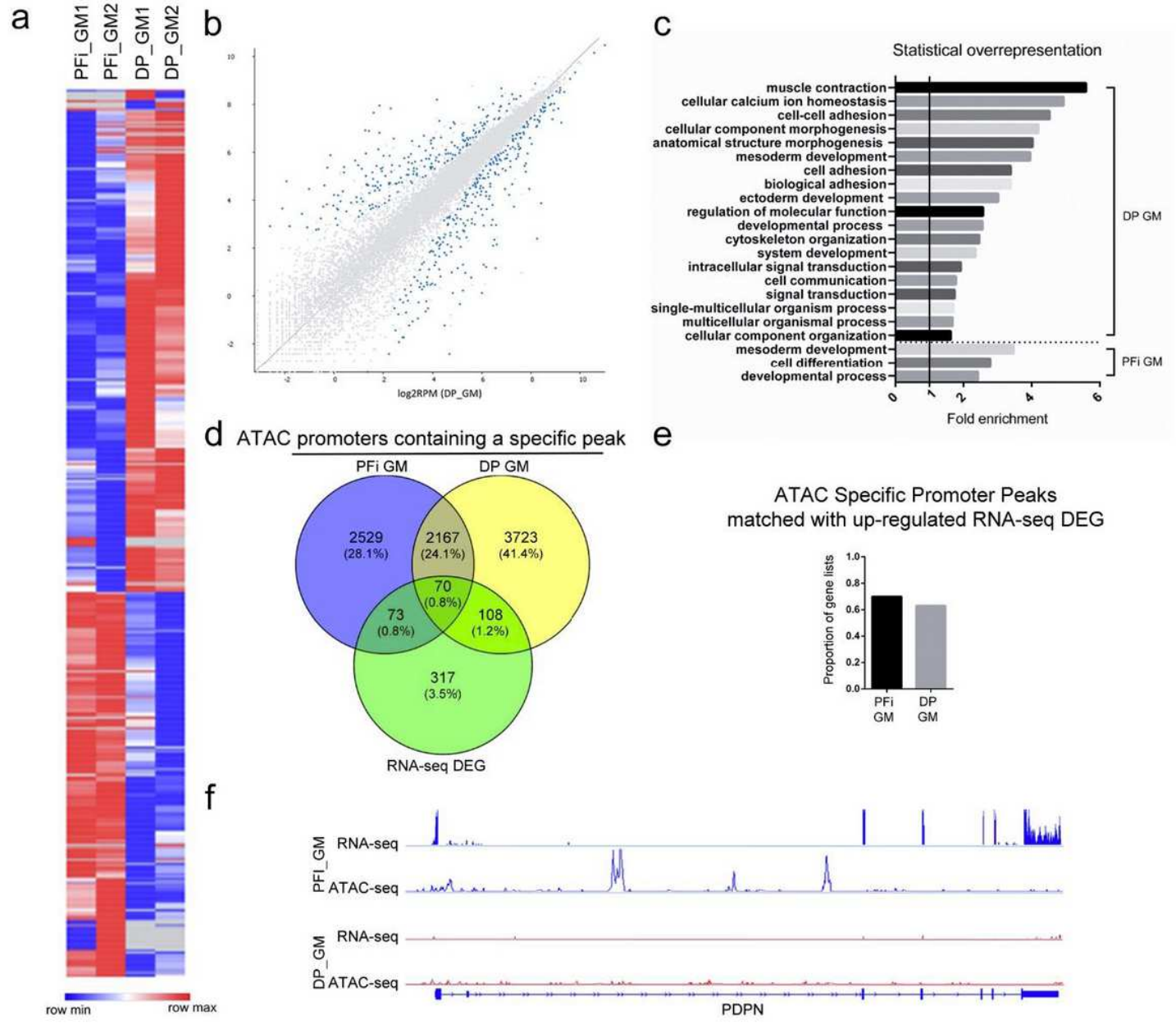

Figure 2

GM Comparison of RNA-seq and ATAC-seq data shows similarities between fibroblast subtypes; a) Heat map displaying differentially expressed genes from RNA-seq analysis; b) Scatter plot showing distribution of RNA-seq differentially expressed genes (blue); c) Gene ontology showing statistically over/under-represented biological processes from upregulated genes in each cell type; d) Venn displaying correlation of ATAC promoters and RNA-seq differentially expressed genes; e) Proportion of ATAC promoters that match with upregulated expression in RNA-seq data; f) Example of RNA-seq differentially

expressed gene matched with identification of an ATAC specific peak within its promoters. Gene shown: PDPN.

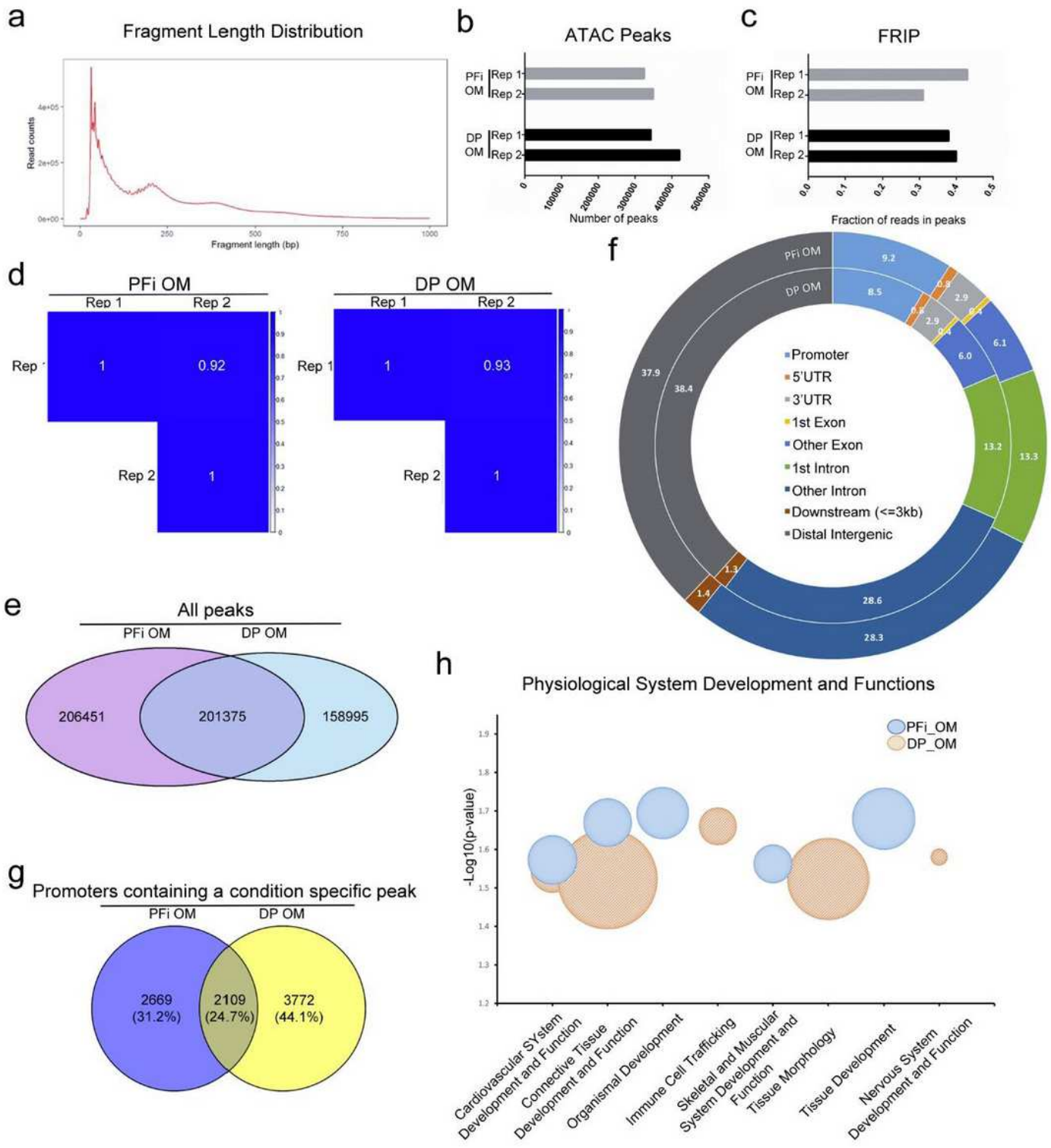

Figure 3

OM Comparison of ATAC-seq reveals divergence of physiological system development and functions; a) ATAC-seq nucleosome banding on PFi OM library; b) Number of ATAC peaks in individual biological replicates; c) FRiP scores from individual biological replicates; d) Correlation matrix; e) Venn diagram

displaying crossover of all ATAC peaks in each condition; f) Peak annotation of specific ATAC peaks on merged samples; g) Venn diagram displaying gene promoters in each condition; h) Gene ontology analysis on ATAC data generated using IPA core analyses. The size of the bubble represents the number of molecules associated within that function.

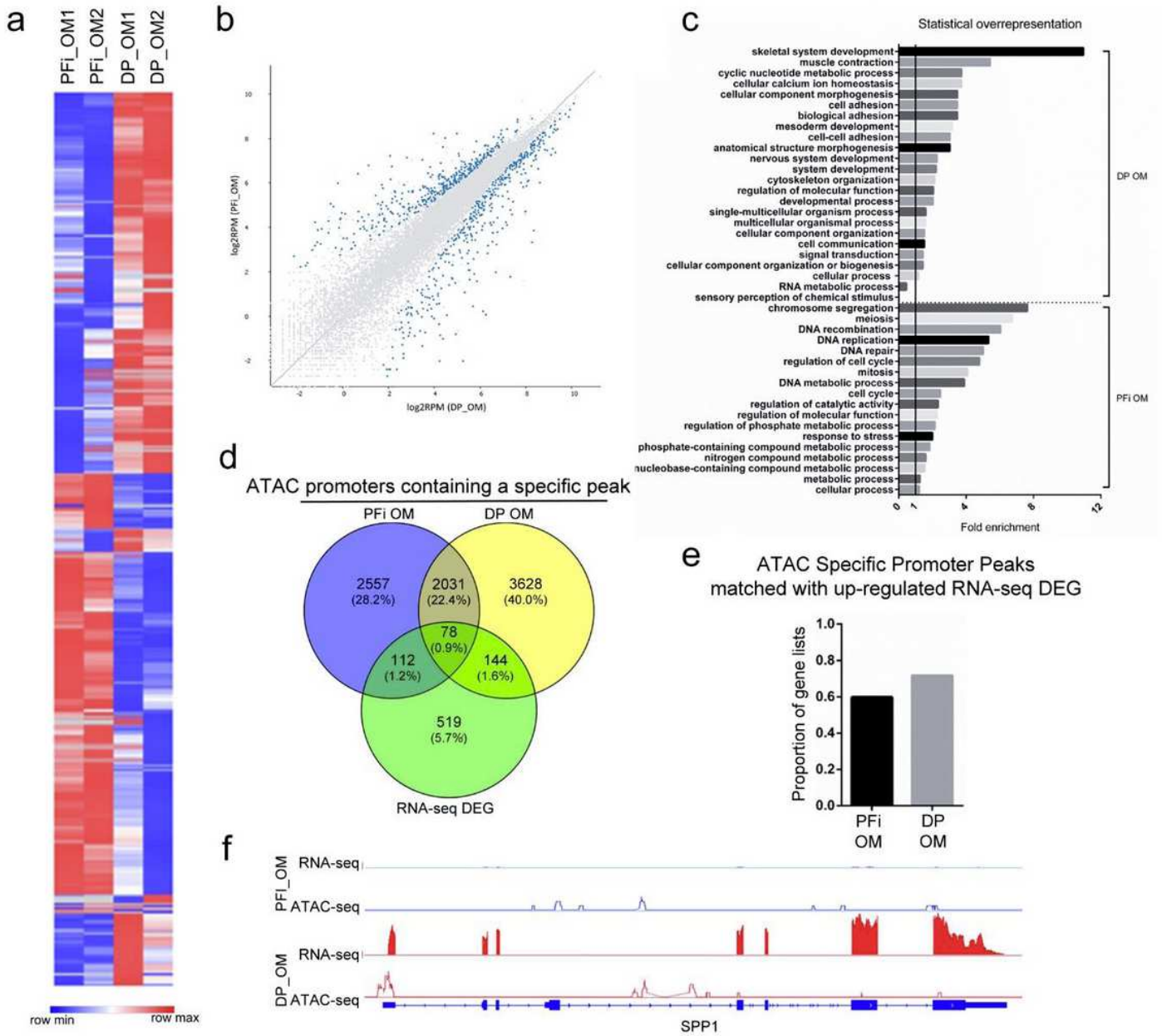

Figure 4

OM Comparison of RNA-seq reveals overrepresentation on skeletal differentiation terms in DP; a) Heat map displaying differentially expressed genes from RNA-seq analysis; b) Scatter plot showing distribution of RNA-seq differentially expressed genes (blue); c) Gene ontology showing statistically over/under-represented biological processes from upregulated genes in each cell type; d) Venn displaying correlation of ATAC promoters and RNA-seq differentially expressed genes; e) Proportion of ATAC promoters that match with upregulated expression in RNA-seq data; f) Example of RNA-seq differentially

expressed gene matched with identification of an ATAC specific peak within its promoters. Gene shown: SPP1.

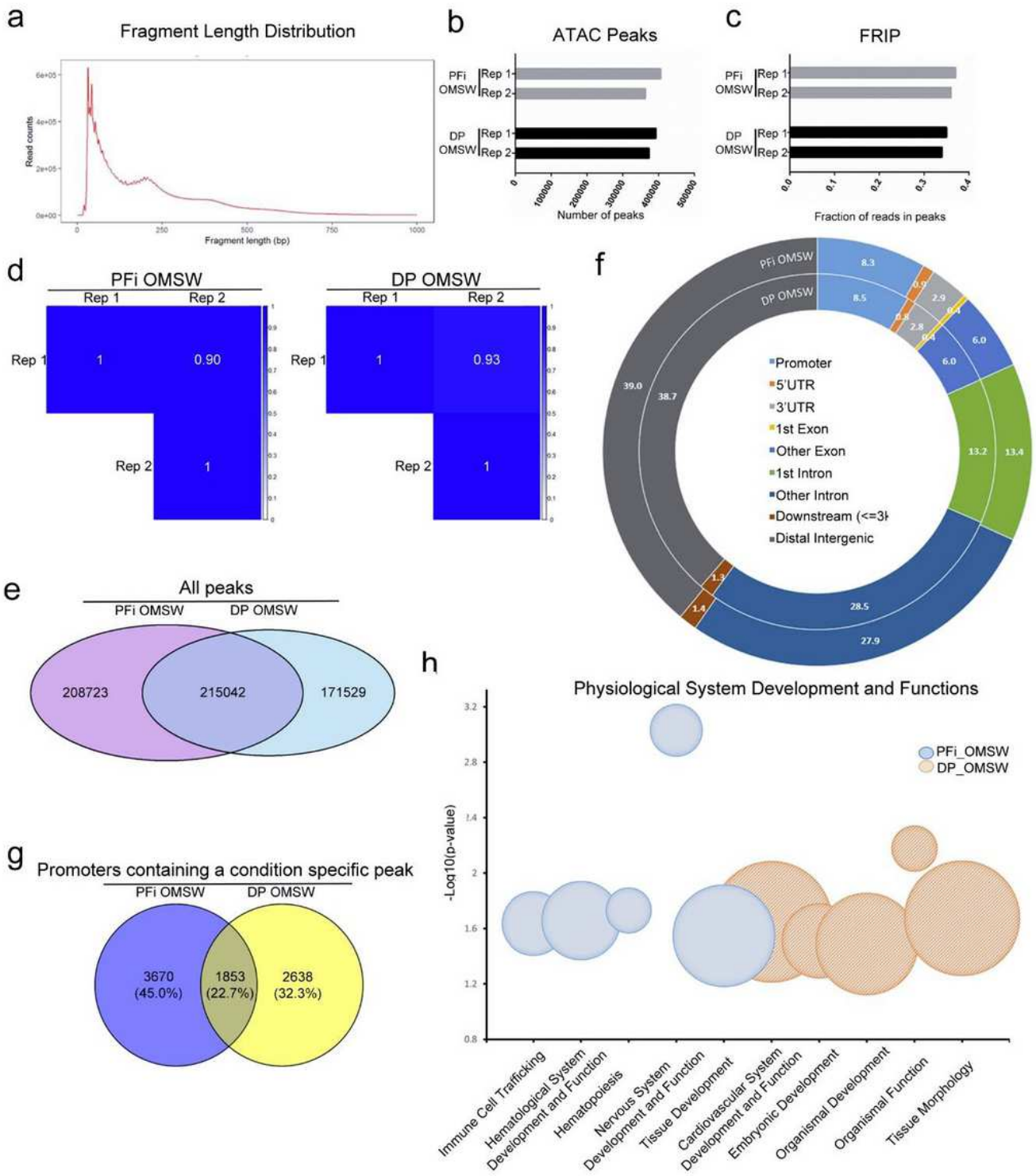

Figure 5

OMSW Comparison uncovers unique chromatin signatures in fibroblasts; a) ATAC-seq nucleosome banding on PFi OMSW library; b) Number of ATAC peaks in individual biological replicates; c) FRiP scores from individual biological replicates; d) Correlation matrix; e) Venn diagram displaying crossover of all

ATAC peaks in each condition; f) Peak annotation of specific ATAC peaks on merged samples; g) Venn diagram displaying gene promoters in each condition; h) Gene ontology analysis on ATAC data generated using IPA core analyses. The size of the bubble represents the number of molecules associated within that function.

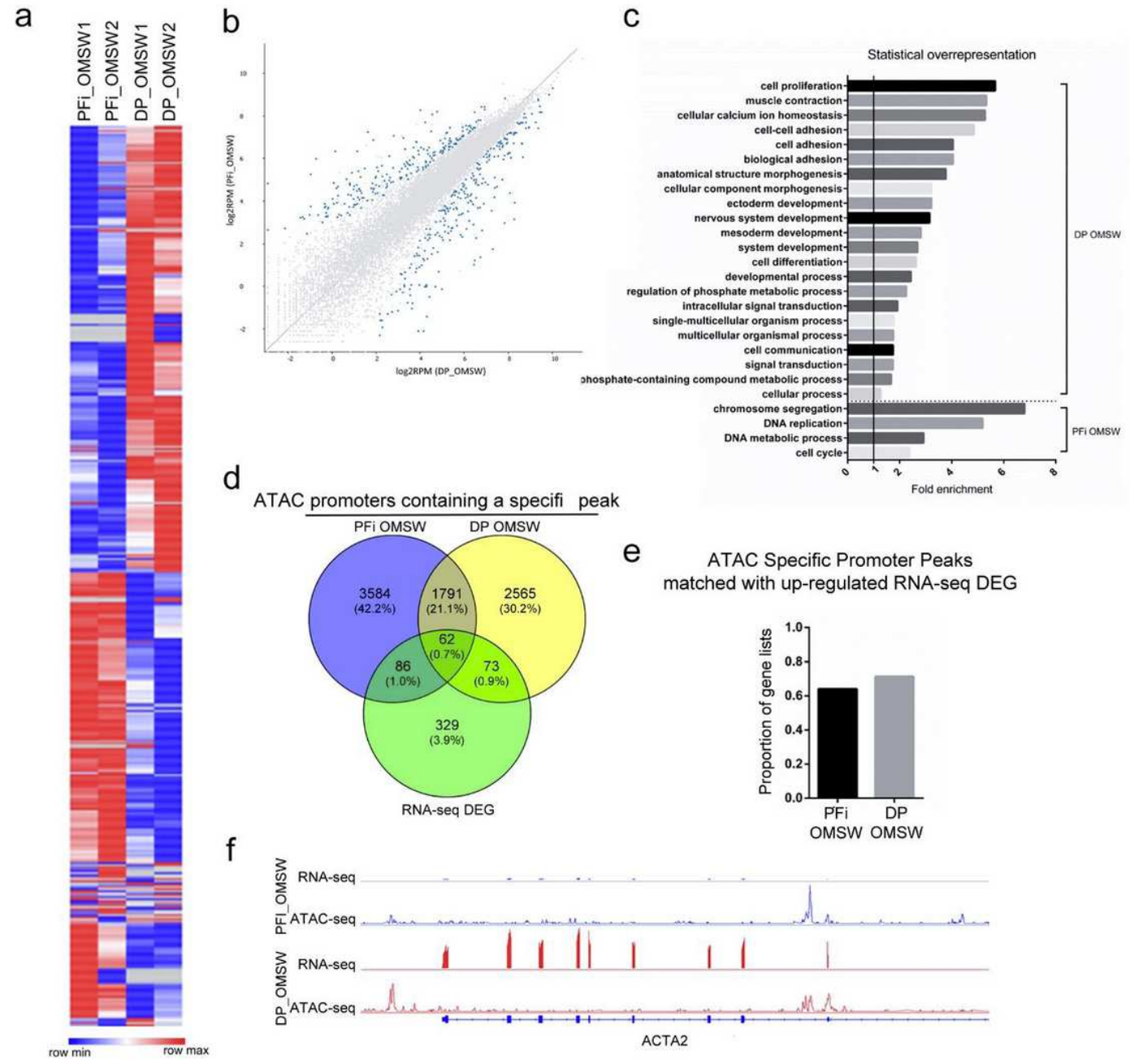

Figure 6

OMSW Comparison uncovers unique chromatin signatures in fibroblasts; a) Heat map displaying differentially expressed genes from RNA-seq analysis; b) Scatter plot showing distribution of RNA-seq differentially expressed genes (blue); c) Gene ontology showing statistically over/under- represented biological processes from upregulated genes in each cell type; d) Venn displaying correlation of ATAC

promoters and RNA-seq differentially expressed genes; e) Proportion of ATAC promoters that match with upregulated expression in RNA-seq data; f) Example of RNA-seq differentially expressed gene matched with identification of an ATAC specific peak within its promoters. Gene shown: ACTA2.

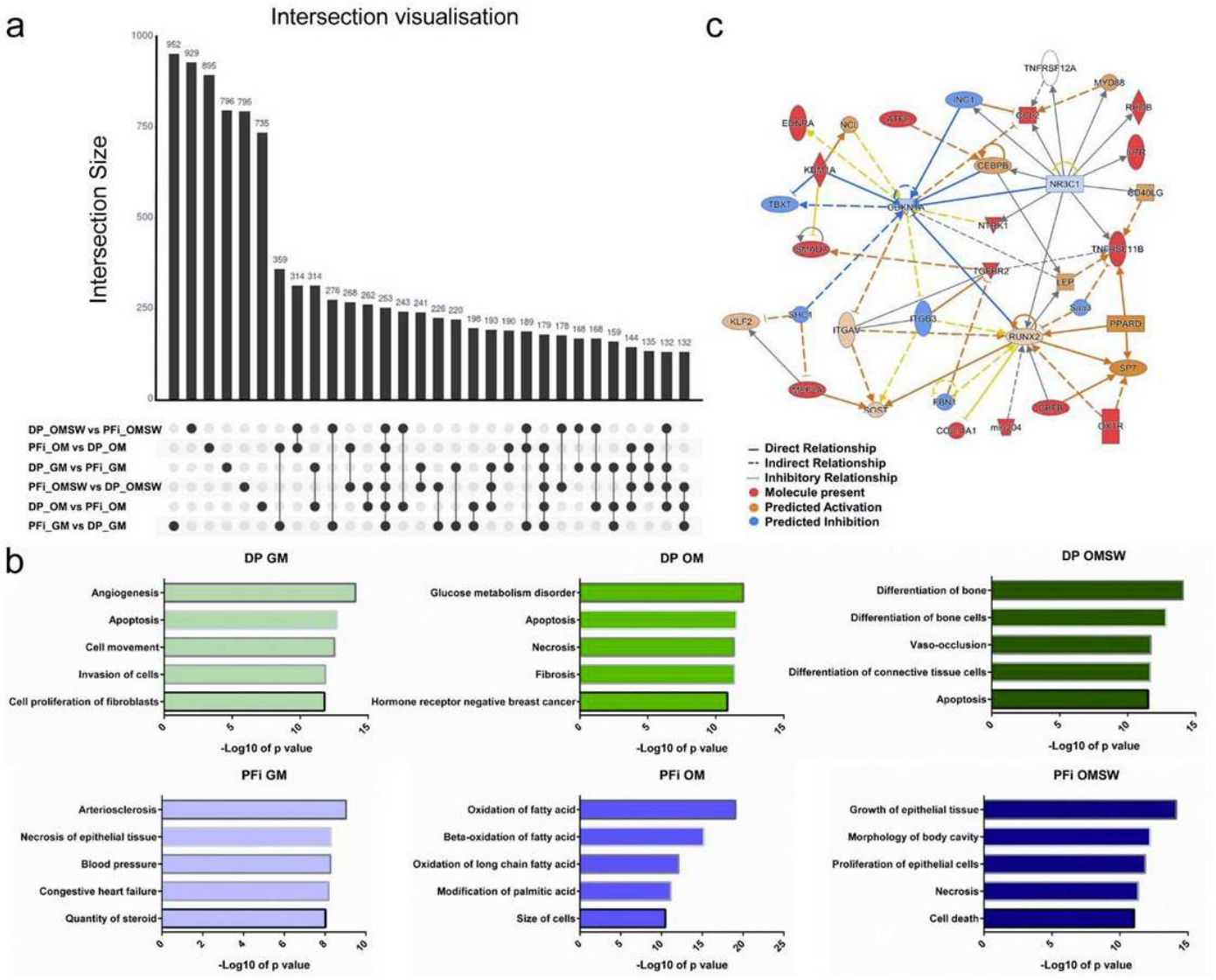

Figure 7

Comparative analysis shows osteogenic enrichment in DP OMSW chromatin profile; a) Intersection visualisation analysis showing the presence of a high number of unique genes in each cell type within each comparison; b) IPA generated network from the unique DP OMSW gene list taken from intersection analysis, showing osteogenic associated interactions; c) Comparison of the top 5 functions associated with the top generated IPA network created using intersection analysis unique gene lists. Only DP OMSW was found to possess osteogenic associated chromatin networks.

Supplementary Files

This is a list of supplementary files associated with this preprint. Click to download.

- SupplementBMCGenomics.pdf